Science of the Total Environment 834 (2022) 155107

Contents lists available at ScienceDirect

Science of the Total Environment

journal homepage: www.elsevier.com/locate/scitotenv

Meteorological influences on daily variation and trend of summertime surface ozone over years of 2015–2020: Quantification for cities in the Yangtze River Delta

Jing Qian, Hong Liao *, Yang Yang, Ke Li, Lei Chen, Jia Zhu

Jiangsu Key Laboratory of Atmospheric Environment Monitoring and Pollution Control, Jiangsu Engineering Technology Research Center of Environmental Cleaning Materials, Collaborative Innovation Center of Atmospheric Environment and Equipment Technology, School of Environmental Science and Engineering, Nanjing University of Information Science & Technology, Nanjing, Jiangsu, China

HIGHLIGHTS

- Meteorology-driven daily and yearly changes in MDA8 O_3 at city scale were studied.
- MLR equations captured 42%–79% of summertime O_3-polluted days over 2015–2020 in cities in YRD.
- 2019–2020 changes in meteorology reduced MDA8 O_3 by 27.7 μg m^{-3} in JJA in YRD.
- RH was the top meteorological driver of daily and yearly variations in summertime MDA8 O_3 in YRD.

GRAPHICAL ABSTRACT

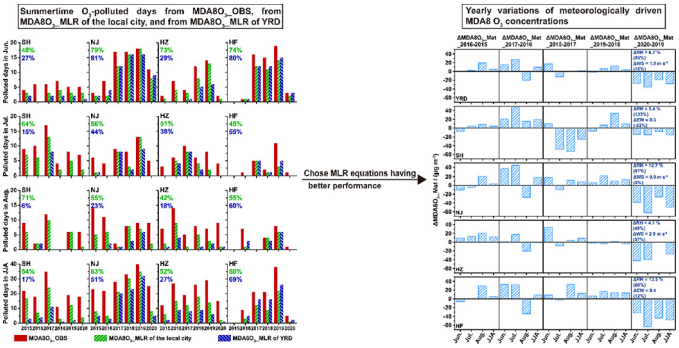

ARTICLE INFO

Editor: Jianmin Chen

Keywords:
Ozone
Meteorological influence
MLR model
Cities in YRD

ABSTRACT

We quantify the meteorological influences on daily variations and trends of maximum daily 8-h average ozone (MDA8 O_3) concentrations by using multiple linear regression (MLR) and Lindeman, Merenda, and Gold (LMG) approaches. Different from previous region-based studies, we pay special attention to meteorological influences at city scale. Over 2015–2019, daily changes in key meteorological parameters could explain 47%–74% of the observed daily variations in summertime MDA8 O_3 concentrations in Yangtze River Delta (YRD) and four cities (Shanghai, Nanjing, Hangzhou, and Hefei), with RH being the top driver. Over years of 2015–2020, daily concentrations of MDA8 O_3 obtained from MLR equations (MDA8O_3_MLR) of the local cities always had better performance than those of YRD. Compared with the observed daily MDA8 O_3 in June–July–August (JJA) over the studied period, daily MDA8O_3_MLR of the local cities (of YRD) had correlation coefficients of 0.73 (0.63), 0.75 (0.74), 0.79 (0.78), and 0.76 (0.73) in Shanghai, Nanjing, Hangzhou, and Hefei, respectively, and the MDA8O_3_MLR of the local cities (of YRD) captured 54% (17%), 63% (51%), 52% (27%) of the observed O_3-polluted days (days with MDA8 O_3 concentration exceeding 160 μg m^{-3}) in Shanghai, Nanjing, and Hangzhou, respectively. The meteorologically driven trends (Trend_Met) in MDA8 O_3 were calculated using the established MLR equations. Over 2015–2019, the observed trends (Trend_Obs) and Trend_Met in MDA8 O_3 were mostly positive in YRD, Nanjing, Hangzhou, and Hefei. In Shanghai, Trend_Obs, Trend_Met, and anthropogenically driven trend (estimated as Trend_Obs minus Trend_Met) of MDA8 O_3 in JJA over 2015–2019 were −1.3, +1.0, and −2.3 μg m^{-3} y^{-1}, respectively, indicating that the emission control measures alleviated O_3 pollution in this city. Our results suggest that it is necessary to establish MLR equations at city scale to account for the role of meteorology in the actions of O_3 pollution control.

* Corresponding author at: No. 219, Ningliu Road, Nanjing 210044, China.
E-mail address: hongliao@nuist.edu.cn (H. Liao).

http://dx.doi.org/10.1016/j.scitotenv.2022.155107
Received 22 November 2021; Received in revised form 14 March 2022; Accepted 3 April 2022
Available online 6 April 2022

1. Introduction

Ground-level ozone (O_3) is an air pollutant generated by photochemical oxidation of nitrogen oxides (NO_x) and volatile organic compounds (VOCs) in the atmosphere in the presence of sunlight. Exposure to high levels of ambient O_3 adversely affects both human health (Yin et al., 2017) and vegetation growth (Yue et al., 2017). In 2013, the Chinese government launched the 'Air Pollution Prevention and Control Action Plan' to improve air quality in China. Since then, $PM_{2.5}$ concentrations have decreased drastically due to stringent emission control measures, while O_3 pollution has been getting worse (Li et al., 2019a, 2019b; Zhai et al., 2019). Understanding the mechanisms for the variations of O_3 is important for O_3 pollution control, especially in the Yangtze River Delta (YRD), one of the largest economic zones in China. According to the 'Environmental and Ecological Status Bulletins in China' (https://www.mee.gov.cn/hjzl/; last access: 8 November 2021), the 90th percentile concentration of the maximum daily 8-h average (MDA8) O_3 averaged over YRD increased largely from 163 μg m^{-3} in 2015 to 180 μg m^{-3} in 2019. The observed summer (June–July–August, JJA) mean MDA8 O_3 concentration increased at a rate of 1.6 ppb y^{-1} over YRD during 2013–2019 (Li et al., 2020).

Concentrations of O_3 are influenced by anthropogenic emissions and meteorological conditions. By using the Weather Research and Forecasting (WRF)-Community Multiscale Air Quality modeling system (CMAQ) model, Liu and Wang (2020) found that the changes in summer MDA8 O_3 in Shanghai due to changes in anthropogenic emissions and meteorology were about +8.9 and +2.1 ppb in 2017 relative to 2013, respectively. They also reported that the changes in wind dominated among meteorological factors that increased MDA8 O_3 in Shanghai over 2013–2017. By using the global 3-D chemical transport model GEOS-Chem, Dang et al. (2021) conducted sensitivity simulations by fixing anthropogenic emissions/meteorological fields at 2012 levels, and found that the changes in anthropogenic emissions and meteorology contributed 0.23 ppb y^{-1} (13%) and 1.47 ppb y^{-1} (84%), respectively, to the trend of simulated MDA8 O_3 in YRD in JJA during the Clean Air Action period of 2012–2017. Their analyses by using the Lindeman, Merenda, and Gold (LMG) method showed that the changes in 10-m wind speed and relative humidity explained, respectively, 40% and 29% of the simulated interannual variations of MDA8 O_3 in JJA over YRD in the simulation with changes in meteorological parameters alone (Dang et al., 2021). By using a stepwise multiple linear regression (MLR) model, Han et al. (2020) showed that meteorology contributed to 41% of the observed increases in summer O_3 averaged over YRD over 2013–2018; the MLR could explain 51% of daily variations in observed surface ozone in which the change in relative humidity was the dominant meteorological driver. Based on the reanalyzed meteorological data and the observed MDA8 O_3 concentrations, Chen et al. (2020a) reported by using a MLR approach that the summer mean anthropogenic-driven and meteorology-driven MDA8 O_3 trends accounted for, respectively, 78% and 22% of the observed MDA8 O_3 trend in YRD over 2014–2018. Li et al. (2020) showed also by a MLR approach that the observed, meteorologically driven, and anthropogenically driven summer MDA8 O_3 trends were 1.7, 0.2, and 1.5 ppb y^{-1}, respectively, in YRD from 2013 to 2017, and the changes in surface air relative humidity, 10-m zonal wind, and 10-m meridional wind explained 80% of monthly variability in MDA8 O_3 in YRD (Li et al., 2019a). These previous studies generally considered the whole of YRD region, which could not account for the spatial heterogeneity in the characteristics of the meteorological influence within the YRD. In addition, these existing studies were mostly focused on the trends of summer mean ozone and did not examine for individual months (i.e., June, July, and August). In JJA, with the march of the East Asian summer monsoon, meteorological conditions for individual months are expected to be different.

In this study, our aims are (1) to quantify the meteorological influence on daily variations and trends of summertime O_3 in the YRD region over 2015–2019, (2) to calculate the relative contributions of key meteorological parameters by developing MLR model and using LMG approach in combination, (3) to compare the characteristics of meteorological influences on summertime (June, July, August, and JJA) MDA8 O_3 concentrations in individual cities with those in the whole of YRD, and (4) to compare the characteristics of meteorological influences in individual months (June, July, and August) with those in the whole summer. The cities of Shanghai, Nanjing, Hangzhou and Hefei were selected as representative cities of the four sub-regions (i.e., Shanghai city, Jiangsu Province, Zhejiang Province, and Anhui Province) in YRD. This paper is organized as follows. Section 2 describes data and methods, including the studied area, observed O_3 concentrations, meteorological data, data preprocessing, MLR model, and LMG method. Section 3.1 presents spatiotemporal variations of observed summertime MDA8 O_3 concentrations in YRD during 2015–2020. Section 3.2 shows key meteorological parameters that drove the daily variations of MDA8 O_3 in YRD and four cities and the performance of MLR equations in different regions/time scales. Sections 3.3 and 3.4 show, respectively, impacts of meteorological parameters on yearly variations and trends of MDA8 O_3 in YRD and four cities. The conclusions and discussions are summarized in Section 4.

2. Data and methods

2.1. Observed concentrations of O_3

This study is focused on 27 cities in the Yangtze River Delta city cluster, including Shanghai, 9 cities (Nanjing, Suzhou, Nantong, Yangzhou, Wuxi, Changzhou, Zhenjiang, Taizhou, and Yancheng) in Jiangsu Province, 9 cities (Hangzhou, Ningbo, Wenzhou, Shaoxing, Huzhou, Jiaxing, Taizhou, Zhoushan, and Jinhua) in Zhejiang Province, and 8 cities (Hefei, Wuhu, Maanshan, Tongling, Anqing, Chuzhou, Chizhou, and Xuancheng) in Anhui Province. The spatial distributions of 27 cities with observed O_3 concentrations are shown in Fig. 1.

The real-time hourly concentrations of observed O_3 for 27 cities of the YRD during 2015–2020 were taken from the public websites of the Chinese Ministry of Ecology and Environment (MEE) (https://www.mee.gov.cn; last access: 8 November 2021) and archived at https://quotsoft.net/air/ (Wang, 2021; last access: 8 November 2021). Until August 2018, O_3 concentrations reported by MEE were in the unit of μg m^{-3} under the standard state of 273 K and 1013 hPa. Starting in September 2018, the reported O_3 concentrations were in the same unit under the reference state of 298 K and 1013 hPa. To facilitate the analysis of long time series, we have converted post-August 2018 O_3 concentrations to the standard state. The MDA8 O_3 concentration was calculated according to the data statistics requirements of Technical regulation for ambient air quality assessment (on trial) (HJ633-2013) (Chinese Ministry of Ecology and Environment, 2013). The 8-h moving averaged concentration was calculated in each day if the valid hourly values were more than 6 h during the 8 h. The MDA8 O_3 concentration was the maximum of the 8-h moving averaged concentrations with more than 14 valid values in each day. The regional (Jiangsu, Zhejiang, Anhui Province, or the YRD) mean MDA8 O_3 was computed if more than 75% of the total city sites in the studied region had valid MDA8 O_3.

2.2. Reanalyzed meteorological data

Meteorological fields for 2015–2020 were obtained from Version 2 of Modern Era Retrospective-analysis for Research and Application (MERRA-2) produced by the NASA Global Modeling and Assimilation Office (GMAO). The MERRA-2 data used in this study have a spatial resolution of 0.5° × 0.625°. The meteorological parameters are listed in Table 1, which include 2-meter air temperature (T2), surface air relative humidity (RH), sea level pressure (SLP), daily total precipitation (PR), daily surface incoming shortwave flux (SW), planetary boundary layer height (PBLH), total column cloud cover (TCC), wind speed at 850 hPa (WS), east-west wind direction indicator at 850 hPa (EW = U/WS, where U is zonal wind at 850 hPa), and north-south wind direction indicator at 850 hPa (NS = V/WS, where V is meridional wind at 850 hPa). Except for relative humidity and wind, for which the temporal resolution is 3 h, other meteorological parameters have a temporal resolution of 1 h.

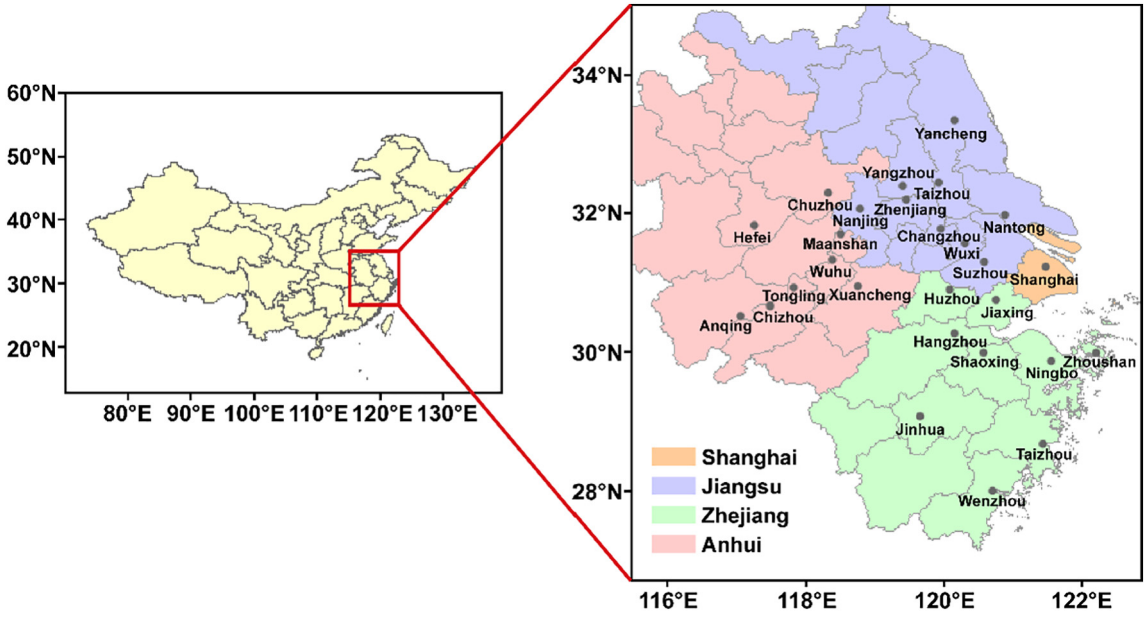

Fig. 1. Spatial distribution of 27 city sites with observed O_3 concentrations in YRD, including Shanghai (covered in orange), 9 cities in Jiangsu Province (purple), 9 cities in Zhejiang Province (green), and 8 cities in Anhui Province (pink).

Both MDA8 O_3 concentrations and meteorological parameters were regionally averaged over each city or YRD to achieve spatial consistency. The MDA8 O_3 concentrations for a city or YRD were obtained by averaging the observed O_3 concentrations from all the monitoring stations in the city or YRD. Considering the horizontal resolution of MERRA-2, the studied regions were assumed to be rectangular, so cities of Shanghai (31.0–31.5°N, 120.7–121.9°E), Nanjing (32.0–32.5°N, 118.2–119.4°E), Hangzhou (29.5–30.5°N, 118.8–120.7°E), and Hefei (31.5–32.0°N, 116.9–117.5°E) covered 6, 6, 12, and 4 grid cells, respectively. The meteorological parameters for a city were calculated by averaging over the grids corresponding to the city. The meteorological parameters for YRD were the average over the 67 grids in the YRD city cluster (27 cities).

2.3. Statistical analysis of the influence of meteorological parameters on MDA8 O_3 concentrations

2.3.1. Meteorological influences on daily variations of MDA8 O_3 concentrations

We aimed to obtain meteorologically driven daily variations of summertime MDA8 O_3 concentrations for years of 2015–2019 considering either the average of YRD or in individual cities of Shanghai, Nanjing, Hangzhou, and Hefei. Stepwise linear regressions between daily observed MDA8 O_3 concentrations and daily meteorological parameters (Table 1) were performed. This approach has been used extensively to describe the relationship between meteorology and air quality (Shen et al., 2015; Otero et al., 2018; Yang et al., 2019). MLR is in the following form:

$$y = \beta_0 + \sum_{k=1}^{N} \beta_k x_k + \varepsilon$$

where y is the observed daily MDA8 O_3 concentrations, x_k is one of the N meteorological parameters listed in Table 1, and β_0 is the intercept term. The regression coefficients β_k for the k-th meteorological parameter was determined by a stepwise method to add and delete terms to obtain the best model fit. The ε is the residual term. Note that we did a screening of the meteorological parameters before reading them into the model. If the correlation coefficient between the observed MDA8 O_3 concentrations and a meteorological parameter in Table 1 was statistically significant at the 95% confidence level in the studied region during 2015–2019, this meteorological parameter would be retained. Stepwise linear regression shows whether an independent variable has significant effect on the dependent variable according to the t-test. If $P < 0.05$, the independent variable was added; otherwise, the independent variable was excluded. The threshold of 10 for the variance inflation factor (VIF) was used to minimize the influences of correlations between the reserved meteorological parameters (Kutner et al., 2004). The adjusted coefficient of determination (R^2) of an equation quantifies the proportion of the dependent variable variability that can be explained by the independent variable variability. In this study, meteorological parameters retained in the MLR equation are called as key meteorological parameters. R^2 represents the proportion of observed daily variations in MDA8 O_3 explained by daily variations in key meteorological parameters during 2015–2019.

Furthermore, to quantify the relative contributions of key meteorological parameters to the observed daily variations in MDA8 O_3 concentrations in the studied regions for years of 2015–2019, the Lindeman, Merenda, and Gold (LMG) method (Grömping, 2006) was applied. The relative contributions were calculated by using daily observed MDA8 O_3 concentrations and key meteorological parameters as inputs of the software package named 'relaimpo'. This approach has been used in many studies to estimate the relative contributions of predictors to the variations of cloud radiative

Table 1
Meteorological parameters considered in the statistical analysis.

Independent variable	Meteorological parameter	Abbreviation
x_1	2-meter air temperature (°C)	T2
x_2	Surface air relative humidity (%)	RH
x_3	Sea level pressure (hPa)	SLP
x_4	Daily total precipitation (mm)	PR
x_5	Daily surface incoming shortwave flux (W m^{-2})	SW
x_6	Planetary boundary layer height (m)	PBLH
x_7	Total column cloud cover (%)	TCC
x_8	Wind speed at 850 hPa (m s^{-1})[a]	WS
x_9	East-west wind direction indicator sinθ (dimensionless)[b]	EW
x_{10}	North-south wind direction indicator cosθ (dimensionless)[b]	NS

[a] Calculated from the horizontal wind vectors (U, V).

[b] θ is the angle of the horizontal surface wind vector counterclockwise from the east. EW and NS are calculated by EW = U/WS and NS = V/WS, respectively, where U, V, and WS are zonal wind (m s^{-1}, positive indicates westerly), meridional wind (m s^{-1}, positive indicates southerly), and wind speed (m s^{-1}) at 850 hPa. EW and NS are dimensionless.

forcing and aerosol optical depth (Xu et al., 2015; Yang et al., 2016; Che et al., 2019).

Once the MLR equation is established using daily parameters (observed MDA8 O_3 concentrations and meteorological parameters) of 2015–2019, daily MDA8 O_3 concentrations in each of the studied regions (YRD, cities of Shanghai, Nanjing, Hangzhou, and Hefei) in summers of 2015–2019 can be obtained by substituting the corresponding daily meteorological parameters into the regression equations, which will be referred to as MDA8O_3_MLR hereafter. Daily MDA8O_3_MLR for summertime of year 2020 will then be 'predicted'. Correlation coefficient (r), mean bias (MB), and normalized mean bias (NMB) between the observed daily MDA8 O_3 concentrations (MDA8O_3_OBS) and daily MDA8O_3_MLR over 2015–2020 were calculated to evaluate the performance of MLR equations.

2.3.2. Meteorological influences on yearly variations and trends of MDA8 O_3 concentrations

Based on the daily MDA8O_3_MLR for 2015–2020, the meteorologically driven yearly changes in MDA8 O_3 concentration (ΔMDA8O_3_Met) can be calculated. It should be noted that ΔMDA8O_3_Met in this paper refers to the change in MDA8 O_3 concentration driven by meteorology relative to the previous year. For example, relative to June of 2019, the ΔMDA8O_3_Met in June of 2020 can be calculated as:

$$\Delta\mathrm{MDA8O_3\_Met} = \mathrm{MDA8O_3\_\bar{MLR}(June,,2020)} - \mathrm{MDA8O_3\_\bar{MLR}(June,2019)} = \frac{1}{D}\sum_{i=1}^{D}\left(\sum_{k=1}^{n}\beta_k x_{k(i)\_June\_2020}\right) - \frac{1}{D}\sum_{i=1}^{D}\left(\sum_{k=1}^{n}\beta_k x_{k(i)\_June\_2019}\right)$$

where D and n represent the days in the month or in JJA and numbers of meteorological parameters retained in the MLR equation, respectively. $x_{k(i)\_June\_2019}$ and $x_{k(i)\_June\_2020}$ represent the k-th meteorological parameter on day i in June of 2019 and in June of 2020, respectively. Relative contribution of each key meteorological parameter to ΔMDA8O_3_Met was quantified by $(\frac{1}{D}\sum_{i=1}^{D}\beta_k x_{k(i)_June_2020} - \frac{1}{D}\sum_{i=1}^{D}\beta_k x_{k(i)_June_2019})/\Delta$MDA8$O_3$_Met.

In addition, the meteorologically driven trend of MDA8 O_3 concentrations (Trend_Met) for years of 2015–2019 was calculated by substituting meteorological data into the developed MLR equation and by linear fitting of the five mean values ($\frac{1}{D}\sum_{i=1}^{D}\left(\sum_{k=1}^{n}\beta_k x_{k(i)\_t\_2015}\right)$, $\frac{1}{D}\sum_{i=1}^{D}\left(\sum_{k=1}^{n}\beta_k x_{k(i)\_t\_2016}\right)$, $\frac{1}{D}\sum_{i=1}^{D}\left(\sum_{k=1}^{n}\beta_k x_{k(i)\_t\_2017}\right)$, $\frac{1}{D}\sum_{i=1}^{D}\left(\sum_{k=1}^{n}\beta_k x_{k(i)\_t\_2018}\right)$, and $\frac{1}{D}\sum_{i=1}^{D}\left(\sum_{k=1}^{n}\beta_k x_{k(i)\_t\_2019}\right)$), where t represents June, July, August, or JJA, and D represents total days in the month or in JJA. The trend driven by the k-th meteorological parameter (Trend_Met$_k$) was calculated as the slope of linear fitting of the five mean values ($\frac{1}{D}\sum_{i=1}^{D}\beta_k x_{k(i)\_t\_2015}$, $\frac{1}{D}\sum_{i=1}^{D}\beta_k x_{k(i)\_t\_2016}$, $\frac{1}{D}\sum_{i=1}^{D}\beta_k x_{k(i)\_t\_2017}$, $\frac{1}{D}\sum_{i=1}^{D}\beta_k x_{k(i)\_t\_2018}$, and $\frac{1}{D}\sum_{i=1}^{D}\beta_k x_{k(i)\_t\_2019}$). Therefore the relative contribution of each key meteorological parameter to the total meteorologically driven trend was quantified by Trend_Met$_k$/Trend_Met. Similarly, the slope of linear fitting of the mean values of observed MDA8 O_3 concentrations for 2015–2019 was defined as the observed trend (Trend_Obs).

2.3.3. Anthropogenic influences on trends of MDA8 O_3 concentrations

Observed trends of MDA8 O_3 concentrations over 2015–2020 were caused by changes in anthropogenic emissions and in meteorology. The removal of the meteorologically driven trend of MDA8 O_3 concentrations from observations leaves a residual trend, which is interpreted as the contribution of anthropogenic emissions. It should be noted that the changes in natural emissions (such as biogenic VOCs and soil NO_x) are considered in meteorological contributions. Such assumption on anthropogenic and meteorological contributions have been used in previous studies such as Li et al. (2019a, 2020), Chen et al. (2020a), and Chen et al. (2020b). Therefore, anthropogenic contributions to Trend_Obs are assumed as Trend_Obs minus Trend_Met.

3. Results

3.1. Spatial and temporal variations in observed MDA8 O_3 concentrations in YRD

Fig. 2 shows the spatial distributions of the summer mean MDA8 O_3 concentrations over YRD from the MEE network for years of 2015–2020. The observed MDA8 O_3 concentrations averaged over YRD kept increasing over 2015–2019 (from 101.8 μg m^{-3} in 2015 to 132.8 μg m^{-3} in 2019) and showed large decreases in 2020 (112.7 μg m^{-3} in 2020). Spatially, Shanghai and Jiangsu Province had the highest MDA8 O_3 concentrations in 2015–2017 and 2020, while Jiangsu and Anhui Provinces were the most polluted regions in 2018 and 2019. Over 2015–2019, the summer mean MDA8 O_3 concentrations in Jiangsu and Anhui Provinces and overall in YRD kept increasing, and those in Shanghai and Zhejiang Province showed fluctuations. During 2015–2019, summer mean MDA8 O_3 concentrations exhibited trends of −1.3, 6.3, 0.4, 16.3, and 7.2 μg m^{-3} y^{-1} in Shanghai, Jiangsu, Zhejiang, Anhui, and YRD, respectively, indicating the fastest increases in O_3 in Jiangsu and Anhui. Although the trend in Shanghai was negative, there were large increases in MDA8 O_3 concentrations in 2017 and 2019. Interestingly, the summer mean O_3 concentrations in 2020 decreased significantly compared with those in 2019, which offers a good opportunity to establish a statistical model using observed O_3 concentrations in 2015–2019 and to predict the changes in MDA8 O_3 concentration in 2020. This can allow one to verify the effectiveness of the statistical model.

Fig. 3 displays the observed yearly variations in seasonal (JJA) or monthly (June, July, and August) mean MDA8 O_3 concentrations over YRD from 2015 to 2020. Generally, MDA8 O_3 concentrations in JJA had an increasing trend from 2015 to 2019 and a sharp decline in 2020. In June, MDA8 O_3 concentrations increased during 2015–2018, and the difference was small between 2018 and 2019. In July, MDA8 O_3 increased over 2015–2017, dropped in 2018 and returned to a high level again in 2019. In August, the concentrations of MDA8 O_3 did not show an obvious trend. Therefore, the yearly variations (or trends) of MDA8 O_3 in different months were inconsistent, which will be examined in detail in the following sections.

3.2. Impacts of meteorological parameters on daily variations of MDA8 O_3 concentrations

3.2.1. Key meteorological parameters that drive the daily variations of MDA8 O_3

The logic of presented results of Section 3.2 is shown in Fig. S1. Here we obtained first the MLR equations between observed MDA8 O_3 concentrations and meteorological parameters as described in Section 2.3.1. The regression equations and key meteorological parameters are summarized in Table 2. Statistically, the percentage of the observed daily variations in MDA8 O_3 explained by variations of key meteorological parameters is represented by the adjusted coefficients of determination (R^2) of MLR, in which the relative contribution from each key meteorological parameter was obtained by LMG method (also described in Section 2.3.1). Fig. 4 shows R^2 and the relative contributions of key meteorological parameters in June, July, August, and JJA of 2015–2019 for YRD and cities of Shanghai, Nanjing, Hangzhou, and Hefei.

Over YRD, the values of R^2 ranged from 0.72 to 0.74 (Fig. 4), indicating that the key meteorological parameters could explain 72%–74% of the observed daily variations in summertime MDA8 O_3 concentrations during 2015–2019. RH was the dominant meteorological parameter, contributing 43%, 79%, 78%, and 82% to the total meteorological influence on daily variations of MDA8 O_3 in June, July, August, and JJA, respectively. There were statistically significant negative correlations between RH and MDA8 O_3 concentrations, with the largest impact on O_3 of −3.7 μg m^{-3} $\%^{-1}$ in YRD in JJA (Table 2). High relative humidity increases the O_3 loss (Johnson et al., 1999; Jacob and Winner, 2009). Considering the whole of YRD, the second most important meteorological parameter that drove the daily variations of MDA8 O_3 was WS in July, August, and JJA, which was negatively correlated with MDA8 O_3 concentrations with regression

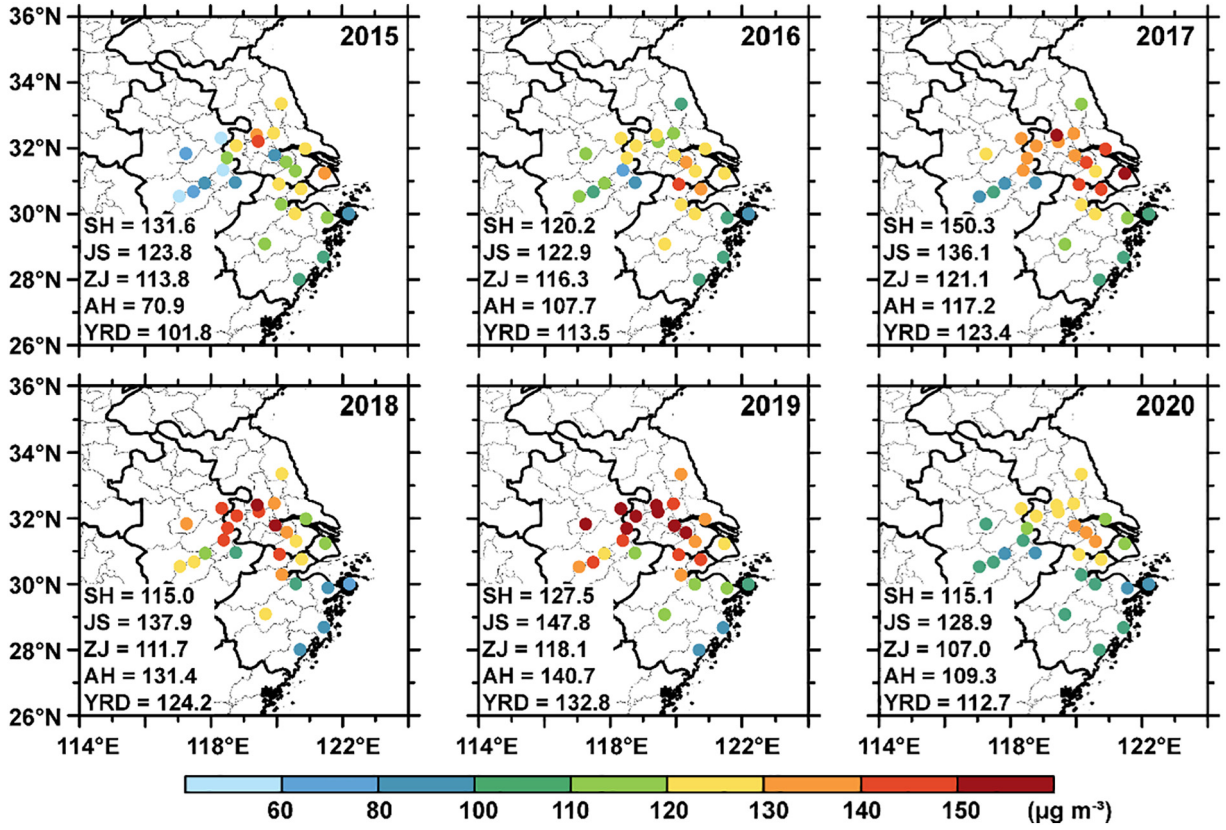

Fig. 2. Spatial distributions of summer (June–July–August, JJA) mean concentrations of observed MDA8 O_3 (μg m^{-3}) at the 27 city sites in YRD for years of 2015–2020. Mean values for Shanghai (SH), Jiangsu (JS), Zhejiang (ZJ), Anhui (AH), and YRD are indicated at the bottom left corner of each panel.

coefficients of -2.3 to -2.8 μg m^{-3} (m s^{-1})$^{-1}$, indicating a dilution effect of winds. The second most important meteorological parameter in YRD was SW for June, which was positively correlated with MDA8 O_3.

In order to compare the characteristics of meteorological effects on daily variations of summertime MDA8 O_3 concentrations in the whole of YRD with those in individual cities within YRD, we selected four cities (i.e., Shanghai, Nanjing, Hangzhou, and Hefei) for analysis. The regression equations and relative contributions of key meteorological parameters in June, July, August, and JJA during the year of 2015–2019 are summarized, respectively, in Table 2 and Fig. 4. In Shanghai, Nanjing, Hangzhou, and Hefei, values of R^2 were 0.47–0.64, 0.50–0.64, 0.62–0.73, and 0.56–0.68 (Fig. 4), respectively, which were lower than those calculated for the whole of YRD.

Over 2015–2019, RH was the top driver for daily variations of summertime MDA8 O_3 concentrations in the four cities, which agreed with that in YRD. The relative contributions of RH to the total meteorological influence

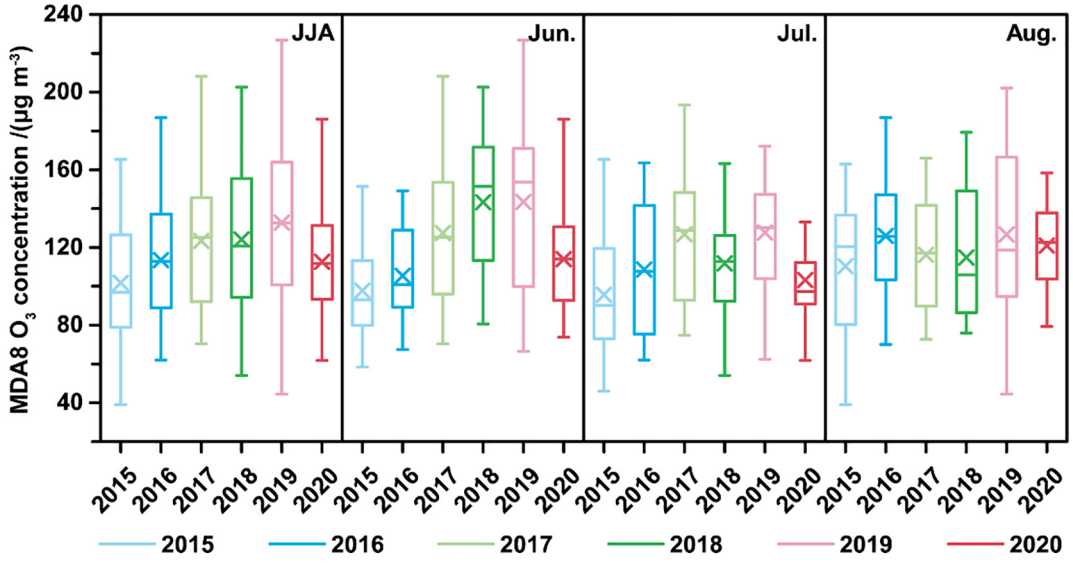

Fig. 3. The observed interannual variations of MDA8 O_3 concentrations (μg m^{-3}) in JJA, June, July, and August averaged over YRD for years of 2015–2020. The boxes enclose 25% percentile, median value, and 75% percentile, the whiskers represent the minimum and maximum values, and crosses represent the average value.

Table 2
Stepwise multiple linear regressions between spatially averaged daily meteorological parameters (shown in Table 1) and observed MDA8 O_3 concentrations in Yangtze River Delta (YRD), Shanghai, Nanjing, Hangzhou, and Hefei in June, July, August, and JJA of 2015–2019. The regression coefficients shown in the equations passed the *t*-test of significance ($P < 0.05$).

Region	Period	Regression equation
YRD	Jun.	MDA8 O_3 = 250.566 − 2.500*RH + 0.005*SW + 0.060*PBLH
	Jul.	MDA8 O_3 = 400.319 − 3.516*RH − 2.292*WS
	Aug.	MDA8 O_3 = 404.287 − 3.562*RH − 2.765*WS
	JJA	MDA8 O_3 = 412.620 − 3.664*RH − 2.335*WS + 3.607*NS
Shanghai	Jun.	MDA8 O_3 = 221.397 − 3.263*RH + 6.908*T2
	Jul.	MDA8 O_3 = 524.243 − 4.994*RH + 26.031*EW
	Aug.	MDA8 O_3 = 361.903 + 35.501*EW − 2.641*RH − 3.068*WS − 0.290*TCC
	JJA	MDA8 O_3 = 433.808 − 3.774*RH + 27.952*EW − 2.183*WS
Nanjing	Jun.	MDA8 O_3 = 248.172 − 3.252*RH + 5.217*T2 − 9.127*EW
	Jul.	MDA8 O_3 = 413.339 − 3.632*RH − 0.381*PR − 1.755*WS
	Aug.	MDA8 O_3 = 262.939 − 2.027*RH − 4.638*WS + 0.009*SW
	JJA	MDA8 O_3 = 354.035 − 3.406*RH − 2.570*WS + 1.773*T2− 6.986*EW
Hangzhou	Jun.	MDA8 O_3 = 263.746 − 2.600*RH + 0.009*SW + 0.059*PBLH − 1.366*WS
	Jul.	MDA8 O_3 = 358.345 − 2.994*RH − 4.086*WS + 0.038*PBLH
	Aug.	MDA8 O_3 = 290.362 − 2.905*RH − 4.481*WS + 3.383*T2
	JJA	MDA8 O_3 = 369.061 − 3.160*RH − 3.412*WS + 0.041*PBLH
Hefei	Jun.	MDA8 O_3 = 174.184 − 2.298*RH − 20.422*EW + 5.457*T2 − 2.121*WS
	Jul.	MDA8 O_3 = 248.715 − 2.795*RH + 2.572*T2 − 11.795*EW
	Aug.	MDA8 O_3 = 150.661 − 2.498*RH + 5.691*T2 − 2.151*WS − 14.200*EW
	JJA	MDA8 O_3 = 289.556 − 2.803*RH − 12.994*EW − 1.697*WS + 1.723*T2

on daily variations of observed MDA8 O_3 were 33%–84%, 41%–80%, 37%–57%, and 56%–72% in Shanghai, Nanjing, Hangzhou, and Hefei, respectively. RH had the largest impacts on MDA8 O_3 in JJA, with regression coefficients of −3.2 and − 2.8 μg m^{-3} $\%^{-1}$ in Hangzhou and Hefei, respectively. In Shanghai and Nanjing, the strongest influences occurred in July (−5.0 and − 3.6 μg m^{-3} $\%^{-1}$, respectively). Except for RH, EW appears frequently as a key meteorological parameter. In Shanghai, the regression coefficient between MDA8 O_3 and EW was positive, which was attributed to the transport of upwind biogenic emissions to Shanghai by southwesterlies that increased MDA8 O_3 concentrations (Chang et al., 2019). In August, considering the daily variation of MDA8 O_3 explained by key meteorological parameters, 42% of the variation was caused by the variation of EW, which was larger than the contribution from the variation of RH (33%) on the basis of the LMG method. On the contrary, the regression coefficient between MDA8 O_3 and EW was negative in Nanjing and Hefei. The southeasterlies brought air mass to pass the highly industrialized and urbanized areas of YRD and eventually reached Nanjing and Hefei (Tu et al., 2007; Xie et al., 2021). The general conclusion for the four cities was that RH, T2, SW, WS, TCC (contributed 9% to daily variation of MDA8 O_3 explained by key meteorological parameters in August in Shanghai), and PR (18% in July in Nanjing) had large effects on the daily variations of MDA8 O_3 concentrations over 2015–2019.

3.2.2. The performances of MLR equations in fitting daily concentrations of $MDA8O_3$_MLR

By substituting the corresponding daily meteorological data into MLR equations in Table 2, daily $MDA8O_3$_MLR were obtained. Fig. 5 compares the daily variations of $MDA8O_3$_OBS with those of $MDA8O_3$_MLR in YRD and four cities for JJA of 2015–2020. The comparisons for individual months of June, July, and August are shown in Figs. S2–S4. In JJA of 2015–2020, the correlation coefficients between $MDA8O_3$_MLR and $MDA8O_3$_OBS were in the range of 0.73–0.83 and MBs (NMBs) were −2.29 (−1.9%), −0.09 (−0.1%), −3.48 (−2.6%), −0.54 (−0.4%) and −2.07 μg m^{-3} (−1.7%), respectively in YRD, Shanghai, Nanjing, Hangzhou, and Hefei. In JJA of different years, the correlation coefficients in YRD, Shanghai, Nanjing, Hangzhou, and Hefei were in the ranges of 0.80–0.89, 0.55–0.78, 0.68–0.83, 0.67–0.83, and 0.63–0.84, respectively, suggesting a fairly good performance of the MLR equations although the fitted O_3 concentrations had small low biases.

Considering the O_3-polluted days (days with MDA8 O_3 concentration exceeding the Chinese Ambient Air Quality (CAAQS) grade II standard of 160 μg m^{-3}), the $MDA8O_3$_MLR could capture, respectively, 34%, 54%, 63%, 52%, and 50% of the observed O_3-polluted days in YRD, Shanghai, Nanjing, Hangzhou, and Hefei in JJA over 2015–2020. It should be noted that $MDA8O_3$_MLR in 2020 were predicted (by using the MLR equations established on the basis of observed MDA8 O_3 and meteorological fields of 2015–2019 (Table 2) as well as 2020 meteorological fields). The r values (NMBs) between $MDA8O_3$_MLR and daily observations over JJA in 2020 were 0.80 (−11.2%), 0.55 (−0.5%), 0.73 (−14.4%), 0.67 (−2.7%), and 0.74 (−10.4%) in YRD, Shanghai, Nanjing, Hangzhou, and Hefei, respectively. $MDA8O_3$_MLR in 2020 captured well the observed decreases in O_3 concentrations in 2020. Compared to 2019, the averaged $MDA8O_3$_OBS ($MDA8O_3$_MLR) dropped by 20.1 (27.7), 12.4 (15.4), 26.5 (49.3), 30.0 (26.9), and 40.6 (47.4) μg m^{-3} in YRD, Shanghai, Nanjing, Hangzhou, and Hefei for JJA of 2020, respectively, suggesting that the changes in meteorological fields had important contributions to the decreases in O_3 and indicating an O_3 increase due to changes in anthropogenic emissions in YRD, Shanghai, Nanjing, and Hefei in 2020. Relative to 2019, concentrations of observed $PM_{2.5}$ dropped by 17%, 1%, 18%, and 18% in YRD, Shanghai, Nanjing, and Hefei for JJA of 2020, respectively. Li et al. (2019a) reported that the decreases in $PM_{2.5}$ was the dominant anthropogenic driver for O_3 increases by slowing down the aerosol sink of hydroperoxy radicals, which then accelerated the O_3 production.

3.2.3. Comparisons of the performances of MLR equations in different regions/time scales

For air quality planning of a specific city in YRD, it would be helpful to obtain a best performance MLR equation to predict daily MDA8 O_3 concentrations ($MDA8O_3$_MLR). There are two concerns here: (1) For MDA8 O_3 in June, July, August, or JJA, should the city use MLR equation fitted using the local daily parameters (observed MDA8 O_3 concentrations and meteorological parameters) or that fitted using the daily parameters averaged over YRD? (2) For MDA8 O_3 in June, July, or August in a specific city, should the city use MLR equation fitted using daily parameters (observed MDA8 O_3 concentrations and meteorological parameters) in this individual month (June, July, or August) or that fitted using daily parameters in the whole of JJA? We address these two issues in this subsection.

Fig. 6 presents the summertime O_3-polluted days obtained from observation, from the MLR equation fitted using the local daily parameters (Table 2), and from the MLR equation fitted using the daily parameters averaged over YRD for cities of Shanghai, Nanjing, Hangzhou, and Hefei in June, July, August, and JJA of 2015–2020. In Shanghai, $MDA8O_3$_MLR of Shanghai and of YRD captured 48%–71% and 6%–27% of the observed O_3-polluted days over 2015–2020, respectively. Furthermore, the better performance of MLR equation of Shanghai than that of YRD held for each year of 2015–2020. Hangzhou has the same situation; the O_3-polluted days in Hangzhou calculated by $MDA8O_3$_MLR of Hangzhou and of YRD accounted for 42%–73% and 18%–38% of observations in 2015–2020, respectively. The similar performance was found in Nanjing in July, August, and JJA. In June, the O_3-polluted days in Nanjing from $MDA8O_3$_MLR of Nanjing and of YRD were 2 (8) and 4 (9) days in 2016 (2020), respectively. In Hefei, the model performance was completely opposite to that in Shanghai and Hangzhou. The proportions of summertime O_3-polluted days captured by the $MDA8O_3$_MLR of Hefei and of YRD were 45%–74% and 55%–80%, respectively, during 2015–2020. In Hefei, the MLR equation of Hefei/of YRD underestimated/overestimated $MDA8O_3$_OBS with an NMB of −1.7%/6.4% in JJA over 2015–2020 (Fig. S5). Thus in Hefei, the high bias in $MDA8O_3$_MLR of YRD explained the capture of more O_3-polluted days than $MDA8O_3$_MLR of Hefei. The similar situation occurred in June, July, and August. Considering the small difference between the proportions of summertime O_3-polluted days captured by $MDA8O_3$_MLR of Hefei and of YRD and the fact that $MDA8O_3$_MLR of Hefei (0.76) had

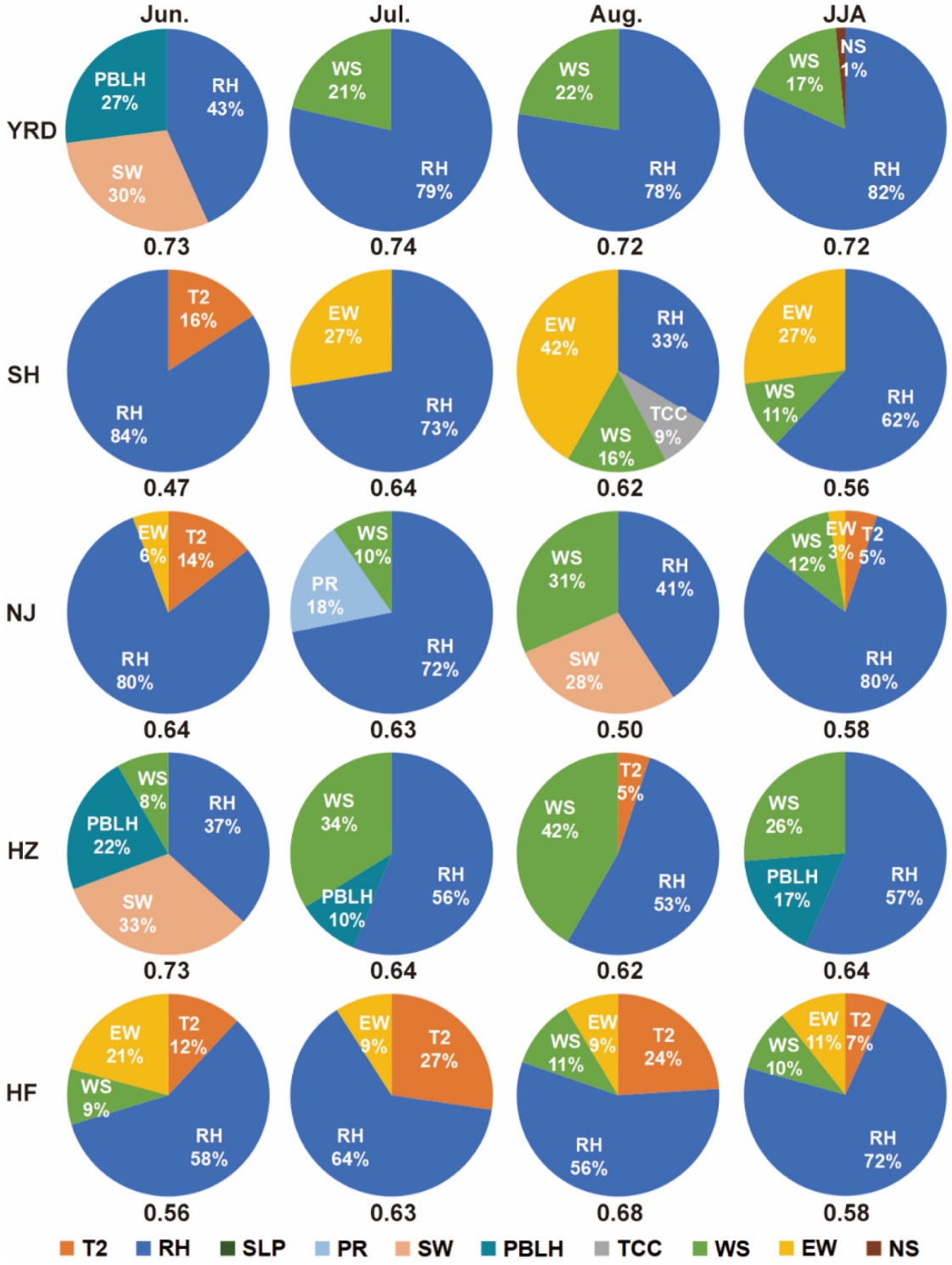

Fig. 4. The estimated relative contribution (%) of each key meteorological variable to the total meteorological impact on observed daily variations of MDA8 O_3 obtained by LMG for June, July, August, and JJA of 2015–2019 in YRD, Shanghai, Nanjing, Hangzhou, and Hefei. See Table 2 for the meteorological parameters retained in MLR equations. The adjusted coefficient of determination of regression (R^2) is indicated at the bottom of each panel.

higher correlation coefficients with MDA8O_3_OBS than MDA8O_3_MLR of YRD (0.73) in JJA (Fig. S5), we think that the exception at Hefei would not compromise the conclusion of this work. Therefore, we suggest MLR equations fitted using the local daily parameters for the application in cities.

Fig. 7 compares the performance of MLR equation fitted using daily parameters of the current month with that of MLR equation fitted using daily parameters of JJA for individual cities of Shanghai, Nanjing, Hangzhou, and Hefei over 2015–2020. In Shanghai, the MLR equation of the current month had better performance than that of JJA in all the months of June, July, and August of 2015–2020; MDA8O_3_MLR of the current month and of JJA captured 48%–71% and 42%–66% of the observed O_3-polluted days respectively. In Nanjing, MDA8O_3_MLR of the current month of June/August captured 79%/55% of the observed O_3-polluted days, which was higher than the ratio of 73%/47% captured by MDA8O_3_MLR of JJA for the same month. However, the O_3-polluted days captured by

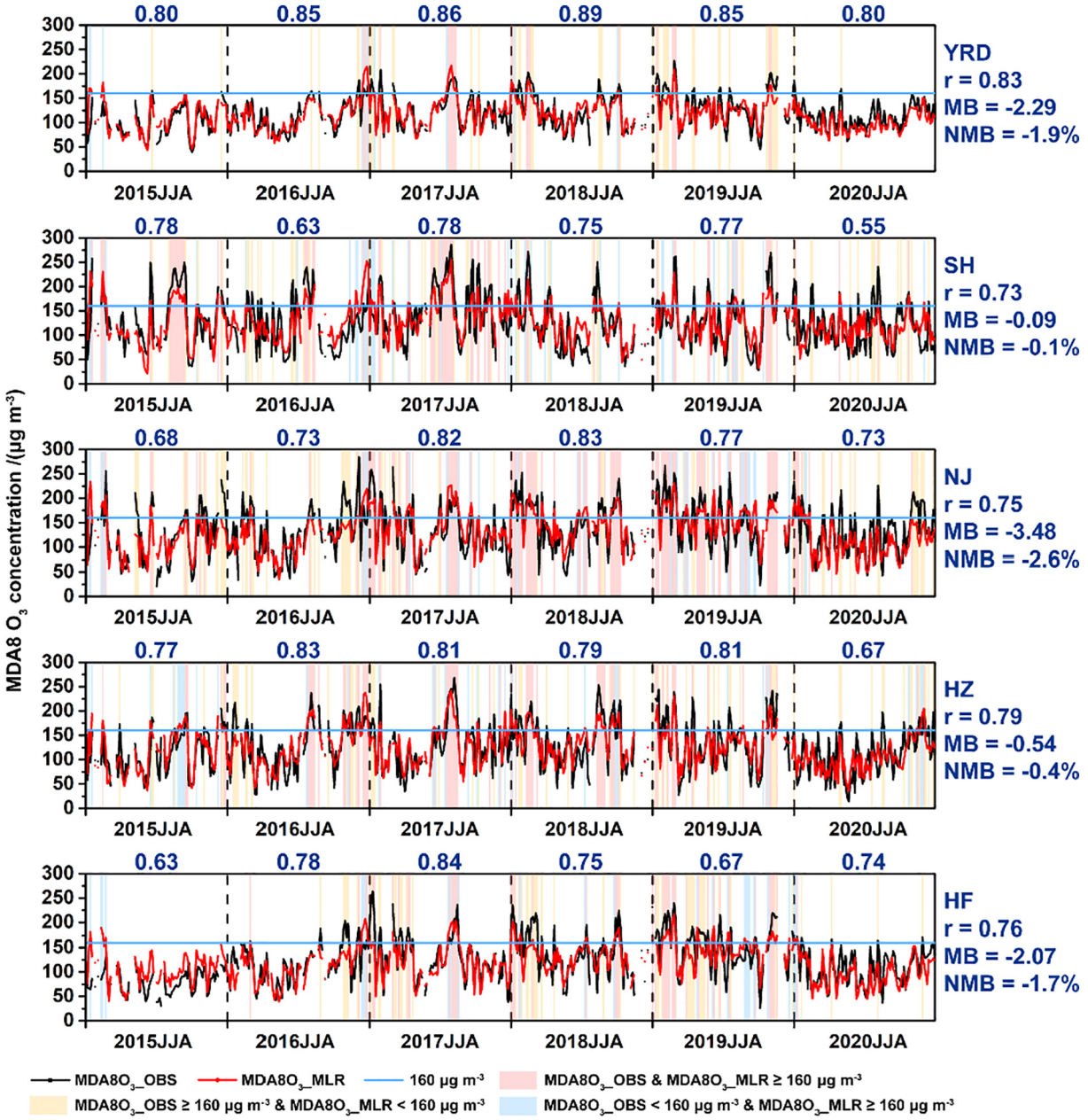

Fig. 5. Time series of daily MDA8 O_3 concentrations (μg m^{-3}) from observation (MDA8O_3_OBS) and from MLR equations (MDA8O_3_MLR) in YRD, Shanghai, Nanjing, Hangzhou, and Hefei in JJA of 2015–2020. MDA8O_3_MLR were calculated by substituting daily meteorological data averaged over YRD or the four cities into the corresponding regression equations in Table 2. The black, red, and blue lines indicate MDA8O_3_OBS, MDA8O_3_MLR, and the Chinese Ambient Air Quality (CAAQS) grade II standard (160 μg m^{-3}), respectively. The light pink, yellow, and blue shades indicate days with MDA8O_3_OBS and MDA8O_3_MLR both exceeding 160 μg m^{-3}, days with only MDA8O_3_OBS exceeding 160 μg m^{-3}, and days with only MDA8O_3_MLR exceeding 160 μg m^{-3}, respectively. Correlation coefficient (r), mean bias (MB), and normalized mean bias (NMB) between MDA8O_3_MLR and MDA8O_3_OBS over 2015–2020 as well as the r values between the two in different years are shown.

MDA8O_3_MLR of JJA were more than those captured by MDA8O_3_MLR of current month in Nanjing in July. The performance of MLR equations of current month was worse than that of JJA in Hangzhou and the performance of these two types of equations was about the same in Hefei. Fig. S6 compares correlation coefficients, MBs, and NMBs between MDA8O_3_OBS and MDA8O_3_MLR of the current month with those between MDA8O_3_OBS and MDA8O_3_MLR of JJA for the four cities. The correlation coefficients of MDA8O_3_MLR of the current month were higher than those of MDA8O_3_MLR of JJA except for Hefei in July, suggesting the use of former approach for cities. For July in Nanjing, July and August in Hangzhou, and July in Hefei, the MBs and NMBs by MDA8O_3_MLR of the current month/of JJA were all negative/positive over 2015–2020, indicating that MDA8O_3_MLR of current month/of JJA underestimated/overestimated the observed MDA8 O_3 concentrations, which led to more O_3-polluted days captured by MLR equations of JJA. To summarize, results above suggest the establishment of MLR equations at city scale on the basis of statistics of current month rather than of JJA.

3.3. Meteorologically driven changes in yearly variations of MDA8 O_3 concentrations

MLR equations fitted using the local daily parameters of the current month have been proved above to be more accurate for cities in the YRD. For these four cities, yearly variations of MDA8 O_3 can be calculated by averaging daily MDA8O_3_MLR over June, July, or August in a specific year from 2015 to 2020 by using MLR equations of the local city and the current

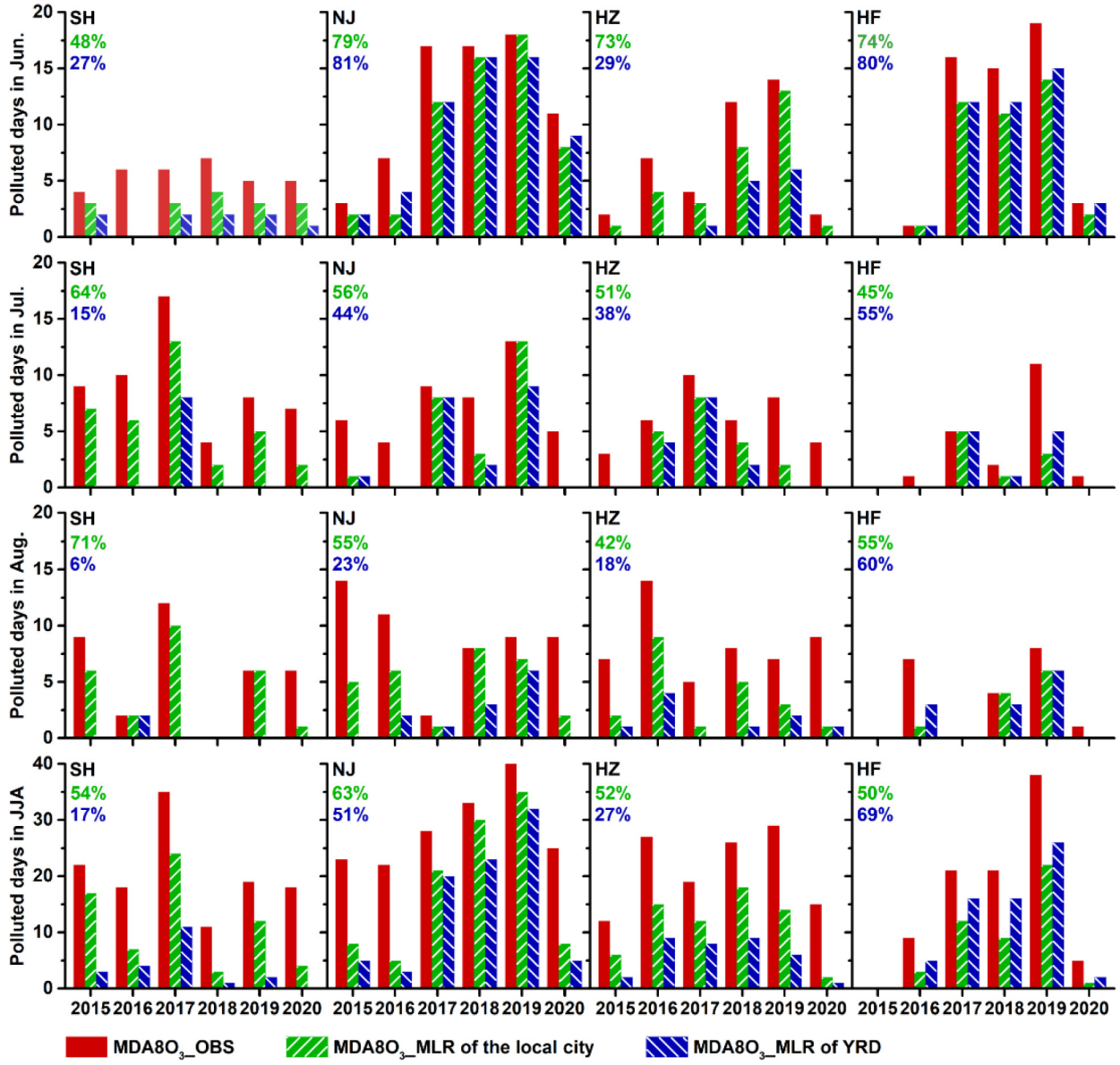

Fig. 6. The summertime O_3-polluted days (days with MDA8 O_3 concentration exceeding 160 μg m^{-3}) from MDA8O_3_OBS, MDA8O_3_MLR of the local cities, and MDA8O_3_MLR of YRD in Shanghai, Nanjing, Hangzhou, and Hefei in June, July, August, and JJA of 2015–2020. The green and blue numbers in each panel indicate the percentages of observed O_3-polluted days captured by MDA8O_3_MLR of the local cities and of YRD over 2015–2020, respectively.

month (Table 2). For later examination of the spatio-temporal heterogeneity of the meteorological influences on yearly variations and trends of MDA8 O_3, we still present the yearly variations of MDA8 O_3 calculated from daily MDA8O_3_MLR from the regression equations of YRD and JJA. Fig. 8 compares yearly variations of MDA8O_3_OBS and MDA8O_3_MLR averaged over YRD and individual cities in June, July, August, and JJA of 2015–2020. The correlation coefficients between yearly MDA8O_3_MLR and MDA8O_3_OBS were generally greater than 0.8 except for in YRD (0.66), Shanghai (0.77), and Nanjing (0.52) in August. MBs (NMBs) were in the range of −2.76 to −1.74 μg m^{-3} (−2.3% to −1.4%), −0.19–0.69 μg m^{-3} (−0.1%–0.5%), −5.47–1.38 μg m^{-3} (−3.9%–1.0%), −0.57–2.03 μg m^{-3} (−0.5%–1.7%), and −4.08–4.34 μg m^{-3} (−3.7%–3.3%), respectively, in YRD, Shanghai, Nanjing, Hangzhou, and Hefei. Yearly variations of MDA8 O_3 calculated from daily MDA8O_3_MLR can capture well the yearly variations in MDA8O_3_OBS with small biases over YRD and four cities. Again, yearly variations of MDA8 O_3 from daily MDA8O_3_MLR of the local city/of the current month had higher correlation coefficients and lower MBs (NMBs) than those of YRD/of JJA in Shanghai, Nanjing, Hangzhou, and Hefei (Figs. S7–S8).

Meteorologically driven yearly changes in MDA8 O_3 concentrations (ΔMDA8O_3_Met_Y2-Y1, indicating MDA8O_3_MLR averaged over year Y2 minus that over year Y1) were calculated (see Section 2.3.2 for details) in YRD, Shanghai, Nanjing, Hangzhou, and Hefei for June, July, August, and JJA of 2015–2020 (Fig. 9). The highest positive ΔMDA8O_3_Met_2016–2015 occurred in August, which were 19.4, 8.0, 20.5, 20.1, and 29.9 μg m^{-3} in YRD, Shanghai, Nanjing, Hangzhou, and Hefei, respectively. The positive ΔMDA8O_3_Met_2017–2016 were the highest/second highest in July/June in YRD, Shanghai, and Nanjing. In Hefei, the meteorological fields resulted in an increase of 32.8/32.4 μg m^{-3} in MDA8 O_3 for June/July in 2017 relative to 2016. Relative to 2017, meteorological fields made a positive/negative contribution to the changes of MDA8 O_3 in June/July in both YRD and individual cities in 2018. In August, largest negative ΔMDA8O_3_Met_2018–2017 (−52.7 μg m^{-3}) occurred in Shanghai among cities, which led to a net negative change in JJA (−25.5 μg m^{-3}). The

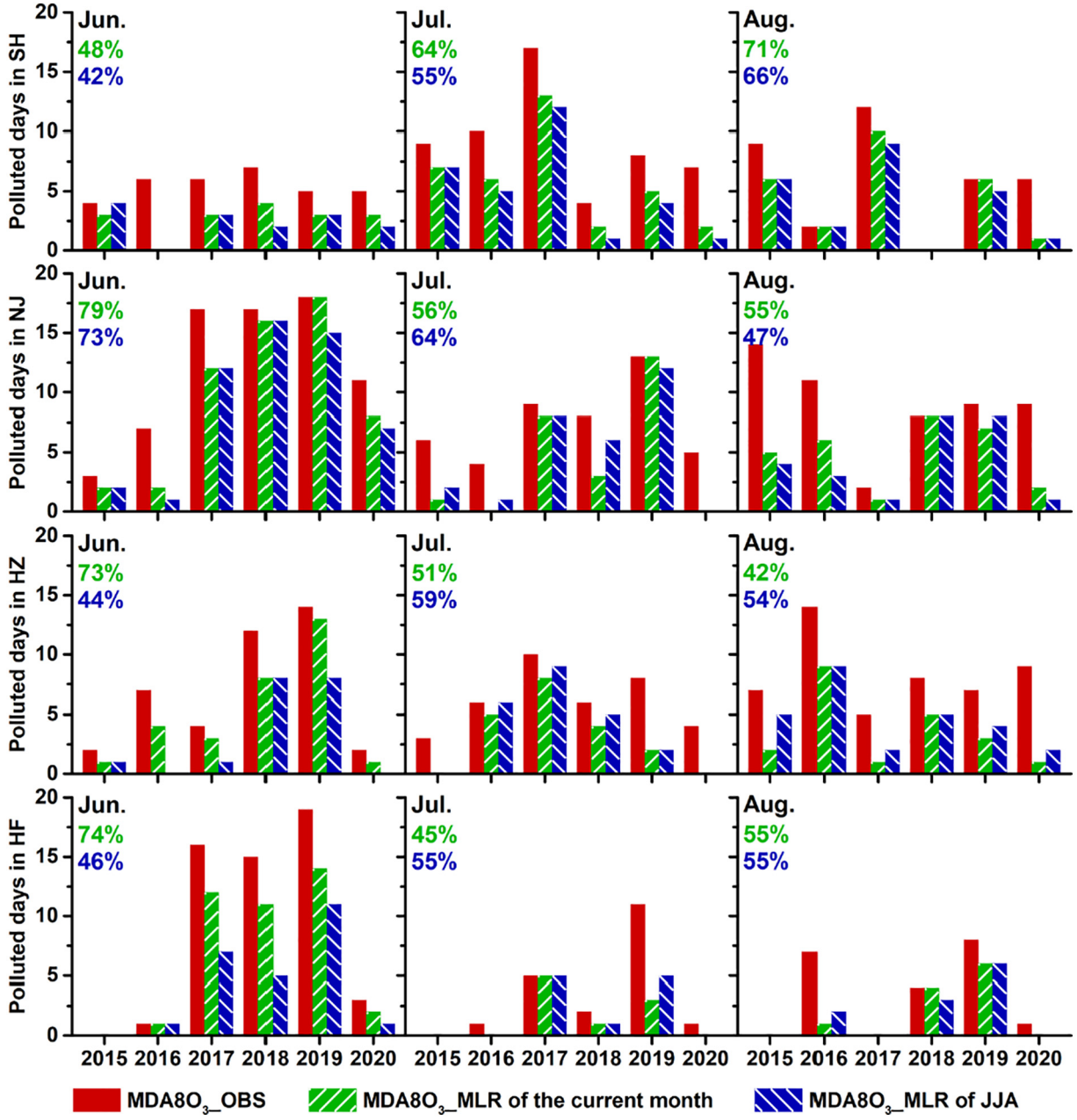

Fig. 7. The summertime O_3-polluted days from MDA8O_3_OBS, MDA8O_3_MLR of the current month, and MDA8O_3_MLR of JJA in Shanghai, Nanjing, Hangzhou, and Hefei in June, July, and August of 2015–2020. The green and blue numbers indicate the percentages of the observed O_3-polluted days captured by MDA8O_3_MLR of the current month and of JJA over 2015–2020, respectively.

ΔMDA8O_3_Met_2019–2018 were all positive in June, July, August, and JJA in Nanjing and Hefei, with the highest increases in July. It is interesting that, relative to 2019, meteorological fields in 2020 led to consistent decreases in MDA8 O_3 in all regions/cities in June, July, August, and JJA. The largest negative ΔMDA8O_3_Met_2020–2019 were in July in YRD (-35.7 μg m^{-3}), Nanjing (-62.3 μg m^{-3}), and Hefei (-62.9 μg m^{-3}), in JJA in Shanghai (-15.4 μg m^{-3}), and in June in Hangzhou (-41.8 μg m^{-3}).

To understand the large meteorologically driven decreases in MDA8 O_3 in 2020 relative to 2019, Fig. 10 shows the spatial distributions of the absolute differences in key meteorological parameters (T2, RH, SW, PBLH, WS, and EW) in June, July, August, and JJA in 2020 relative to 2019. These meteorological parameters were taken from MERRA-2 reanalyzed data with a horizontal resolution of 0.5° × 0.625°. Over 2019–2020, T2 either increased or decreased (in the range of -3.0 to $+3.0$ °C) in the studies regions. RH increased from 2019 to 2020 by 7.3, 7.9, 5.1, and 6.7% in June, July, August, and JJA, respectively, as the values were averaged over YRD, which had an effect of reducing MDA8 O_3 (Gong and Liao, 2019). In addition, decreases in summertime SW and PBLH and increases in summertime WS and EW occurred in almost the entire YRD region over 2019–2020.

The relative contributions of above meteorological parameters to ΔMDA8O_3_Met_2020–2019 can be quantified as described in Section 2.3.2. The top two meteorological parameters that contributed to ΔMDA8O_3_Met_2020–2019 averaged over JJA are shown in the right most column of Fig. 9. Considering the average over JJA and YRD, the increases in RH by 6.7% and in WS by 1.9 m s^{-1} from 2019 to 2020 contributed, respectively, 89% and 16% to the ΔMDA8O_3_Met_2020–2019 of -27.7 μg m^{-3}. Similarly, increases in RH and WS accounted for 87%/48% and 5%/37% of the meteorology-driven decrease averaged over JJA in 2020 relative to 2019 in Nanjing/Hangzhou, respectively. In Shanghai,

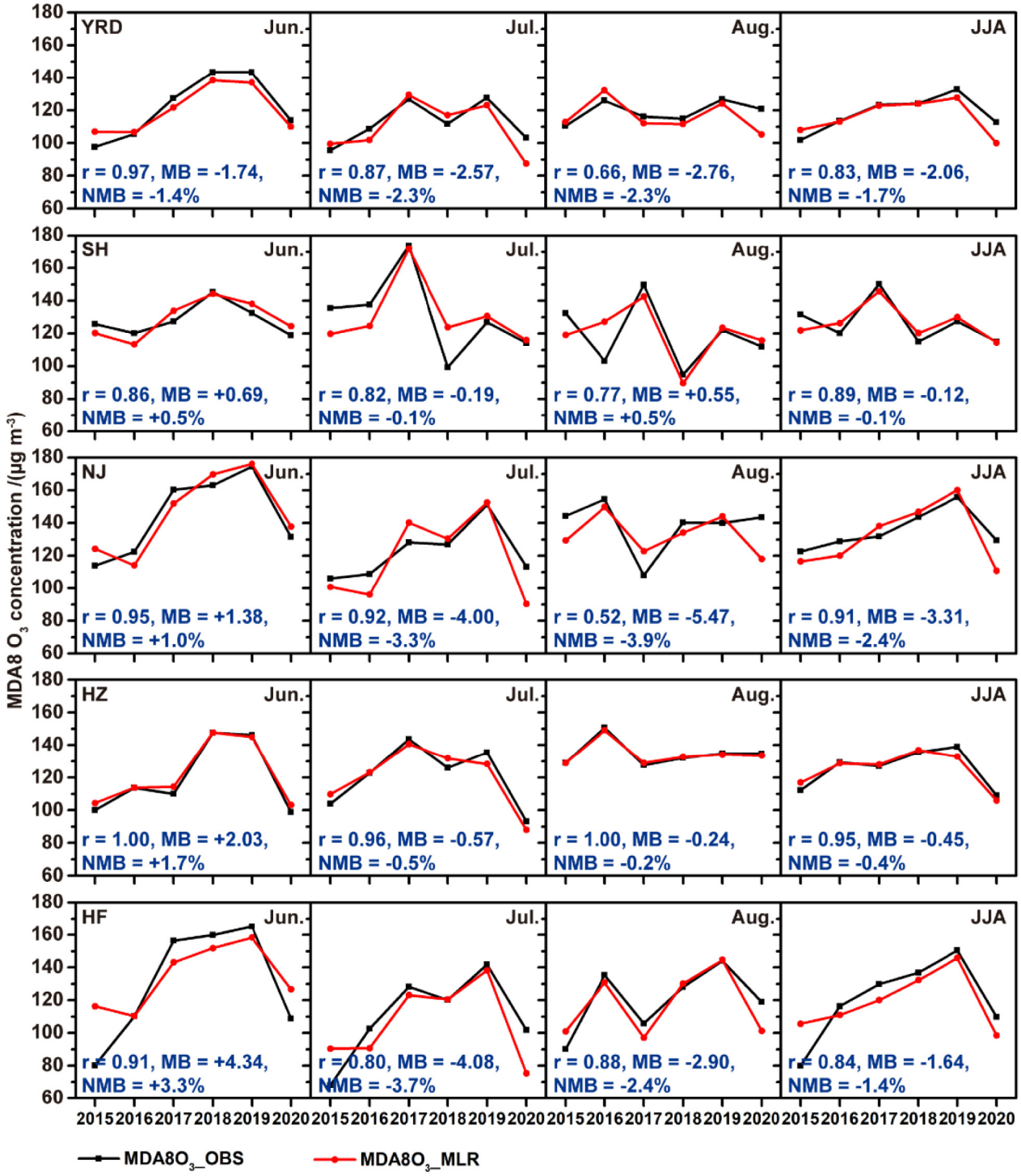

Fig. 8. Yearly variations of monthly (June, July, and August) and seasonal (JJA) mean MDA8O_3_OBS and MDA8O_3_MLR in YRD, Shanghai, Nanjing, Hangzhou, and Hefei from 2015 to 2020. For the four cities, yearly variations of MDA8 O_3 were calculated by averaging daily MDA8O_3_MLR over June, July, or August in a specific year from 2015 to 2020 by using MLR equations of the local city and the current month (Table 2). The black and red lines indicate values from MDA8O_3_OBS and MDA8O_3_MLR, respectively. r, MB, and NMB between yearly MDA8O_3_OBS and MDA8O_3_MLR of 2015–2020 are shown at the bottom left corner of each panel.

increases in RH and EW were the top two drivers, contributing 133% and −62% to the negative ΔMDA8O_3_Met_2020–2019 for JJA, respectively, due to the positive regression coefficient between MDA8 O_3 and EW. In Hefei, increases in RH and EW made contributions of 80% and 12% to the meteorologically driven decreases in MDA8 O_3 concentrations averaged over JJA in 2020 relative to 2019.

3.4. Meteorologically driven trends of MDA8 O_3 concentrations

The observed and meteorologically driven trends (Trend_Obs and Trend_Met) of summertime MDA8 O_3 concentrations in YRD, Shanghai, Nanjing, Hangzhou, and Hefei over 2015–2019 are shown in Fig. 11. Trend_Met for years of 2015–2019 was calculated as the slope obtained

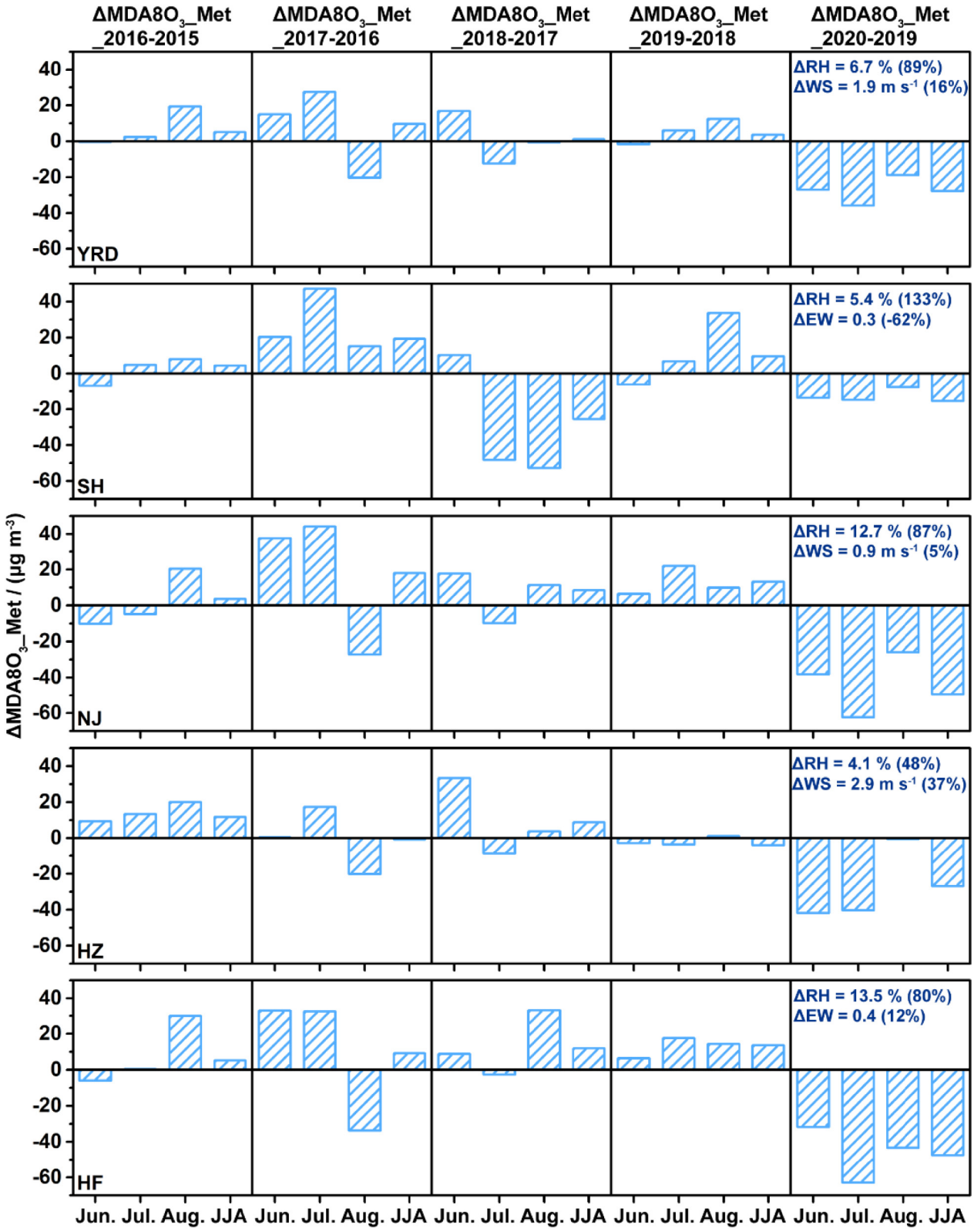

Fig. 9. Meteorologically driven yearly variations of MDA8 O_3 concentrations (μg m^{-3}) for June, July, August, and JJA in YRD, Shanghai, Nanjing, Hangzhou, and Hefei. In the right most column, the absolute differences (2020–2019) in two most dominant meteorological parameters averaged over JJA as well as their percentage contribution to ΔMDA8O_3_Met_2020–2019 were also shown for YRD, Shanghai, Nanjing, Hangzhou, and Hefei. Units of ΔRH and ΔWS are % and m s^{-1}, respectively. ΔEW is dimensionless.

by linear fitting of the five mean values ($\frac{1}{D}\sum_{i=1}^{D}\left(\sum_{k=1}^{n}\beta_k x_{k(i)\_t\_2015}\right)$, $\frac{1}{D}\sum_{i=1}^{D}\left(\sum_{k=1}^{n}\beta_k x_{k(i)\_t\_2016}\right)$, $\frac{1}{D}\sum_{i=1}^{D}\left(\sum_{k=1}^{n}\beta_k x_{k(i)\_t\_2017}\right)$, $\frac{1}{D}\sum_{i=1}^{D}\left(\sum_{k=1}^{n}\beta_k x_{k(i)\_t\_2018}\right)$, and $\frac{1}{D}\sum_{i=1}^{D}\left(\sum_{k=1}^{n}\beta_k x_{k(i)\_t\_2020}\right)$) (see Section 2.3.2 for more details). Over YRD, for June, July, August, and JJA, the Trend_Obs were +12.9, +6.7, +2.2, and +7.2 μg m^{-3} y^{-1}, respectively, and the estimated meteorological driven trends were +9.2 (71% of the observed trend), +6.2 (93%), +0.2 (9%), and +5.0 (69%)

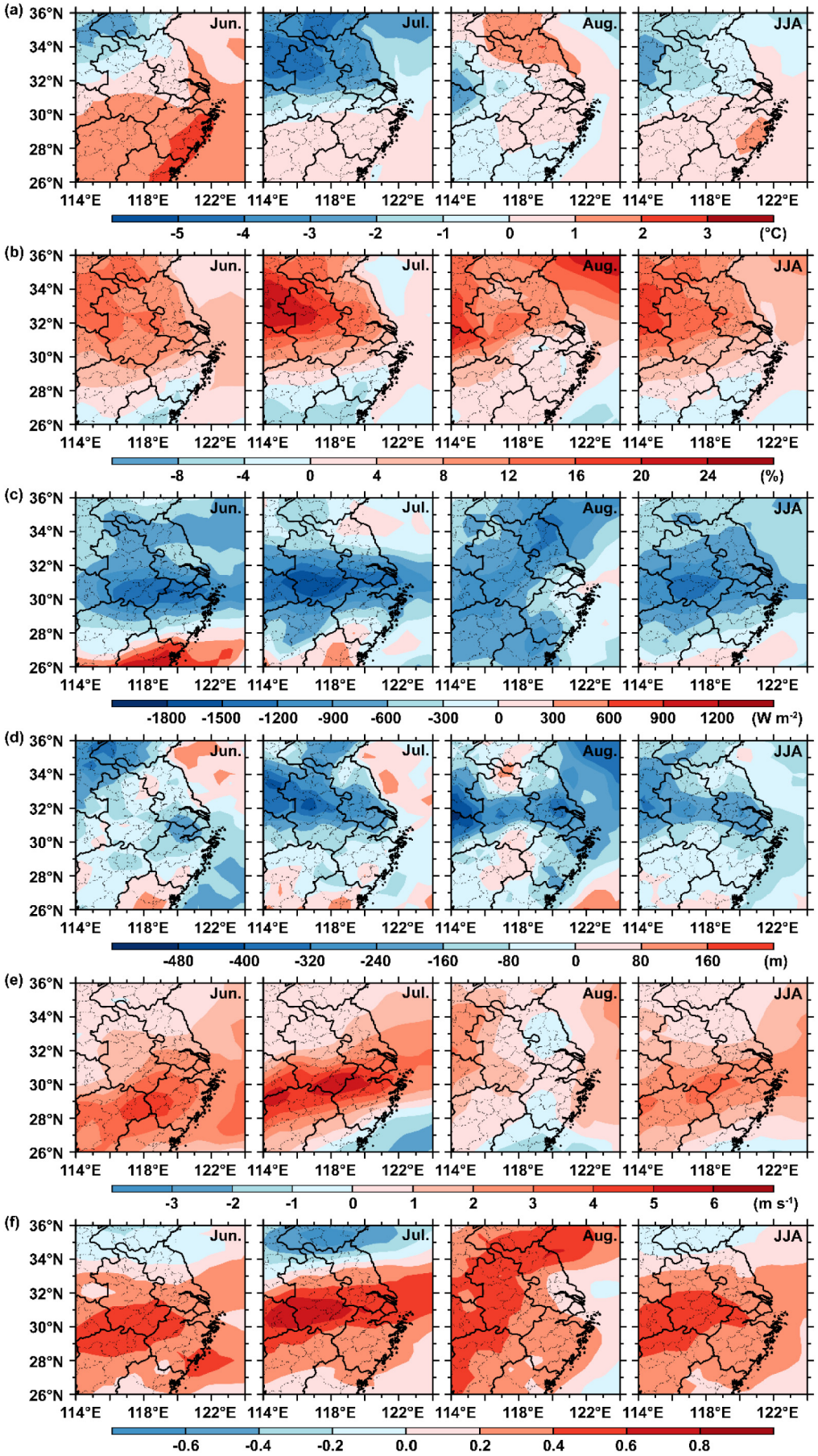

Fig. 10. Spatial distributions of absolute differences in monthly (June, July, and August) and seasonal (JJA) mean (a) T2 (°C), (b) RH (%), (c) SW (W m^{-2}), (d) PBLH (m), (e) WS (m s^{-1}), and (f) EW (dimensionless) over YRD in 2020 relative to 2019.

μg m^{-3} y^{-1}, respectively. The upward trends were the largest in June and smallest in August. In June, July, and JJA from 2015 to 2019, the increasing trends were mainly attributed to the changes in meteorological fields. Considering JJA and YRD, the changes in meteorological fields are estimated to contribute 69% to Trend_Obs over 2015–2019 in our study, which is larger than the meteorological contribution of 44% over 2013–2019 reported by Li et al. (2020) by using a MLR approach, and is smaller than the meteorological contribution of 84% over 2012–2017 reported by Dang et al. (2021) by using the GEOS-Chem model. Further investigation showed that the decreases in RH (−2.0, −1.3, −0.2, and −1.2% y^{-1}) was the most dominant meteorological parameter, contributing 55%, 70%, 488%, and 84% to Trend_Met in YRD for June, July, August, and JJA over 2015–2019, respectively. In August, the Trend_Obs and Trend_Met were +2.2 and +0.2 μg m^{-3} y^{-1}, respectively; decreases in RH (−0.2% y^{-1}) and increases in WS (+0.3 m s^{-1} y^{-1}) explained 488% and −388% of the Trend_Met, respectively in YRD over 2015–2019.

Fig. 11(b) presents Trend_Obs and Trend_Met in Shanghai, Nanjing, Hangzhou, and Hefei for June, July, August, and JJA over 2015–2019. In Shanghai, the Trend_Obs was positive only for June, with Trend_Met making a contribution of 174% over 2015–2019. The situations of Trend_Obs and Trend_Met over 2015–2019 in Nanjing and Hangzhou were similar to those in YRD except in August, when the Trend_Obs were negative in both cities. In Hefei, Trend_Obs and Trend_Met of 2015–2019 were all positive. The upward Trend_Obs and Trend_Met of MDA8 O_3 were both the largest in June in four cities, similar to those in YRD. In most instances, RH was the most dominant meteorological parameter of summertime Trend_Met in four cities. In addition, WS was the top driver of Trend_Met for a certain month in a certain city (August in Shanghai as well as July and August in Hangzhou) during 2015–2019.

Assuming that anthropogenic contributions to Trend_Obs can be obtained by Trend_Obs minus Trend_Met (see Section 2.3.3 for more details). Over 2015–2019, changes in anthropogenic emissions always made a positive contribution to the positive summertime Trend_Obs in YRD (7%–91% of the observed trend), Hangzhou (9%–32% in June, July, and JJA), and Hefei (14%–43%). Li et al. (2019a) confirmed that decrease of $PM_{2.5}$ slowed down the aerosol sink of hydroperoxy (HO_2) radicals, which stimulated ozone production over 2013–2017 by Geos-Chem model. In Shanghai and Nanjing, changes in anthropogenic emission were suspected to suppress summertime MDA8 O_3 increases during the five years. The largest negative anthropogenically driven trend of −7.6/−3.6 μg m^{-3} y^{-1} occurred in July/August in Shanghai/Nanjing over 2015–2019.

In summary, Trend_Obs and Trend_Met of June, July, August, and JJA during the year of 2015–2019 over YRD, Nanjing, Hangzhou, and Hefei were mostly positive. RH was very often the top driver of Trend_Met in YRD and individual cities for 2015–2019. The statistics showed that emission control measures in Shanghai and Nanjing inhibited ozone increases over 2015–2019.

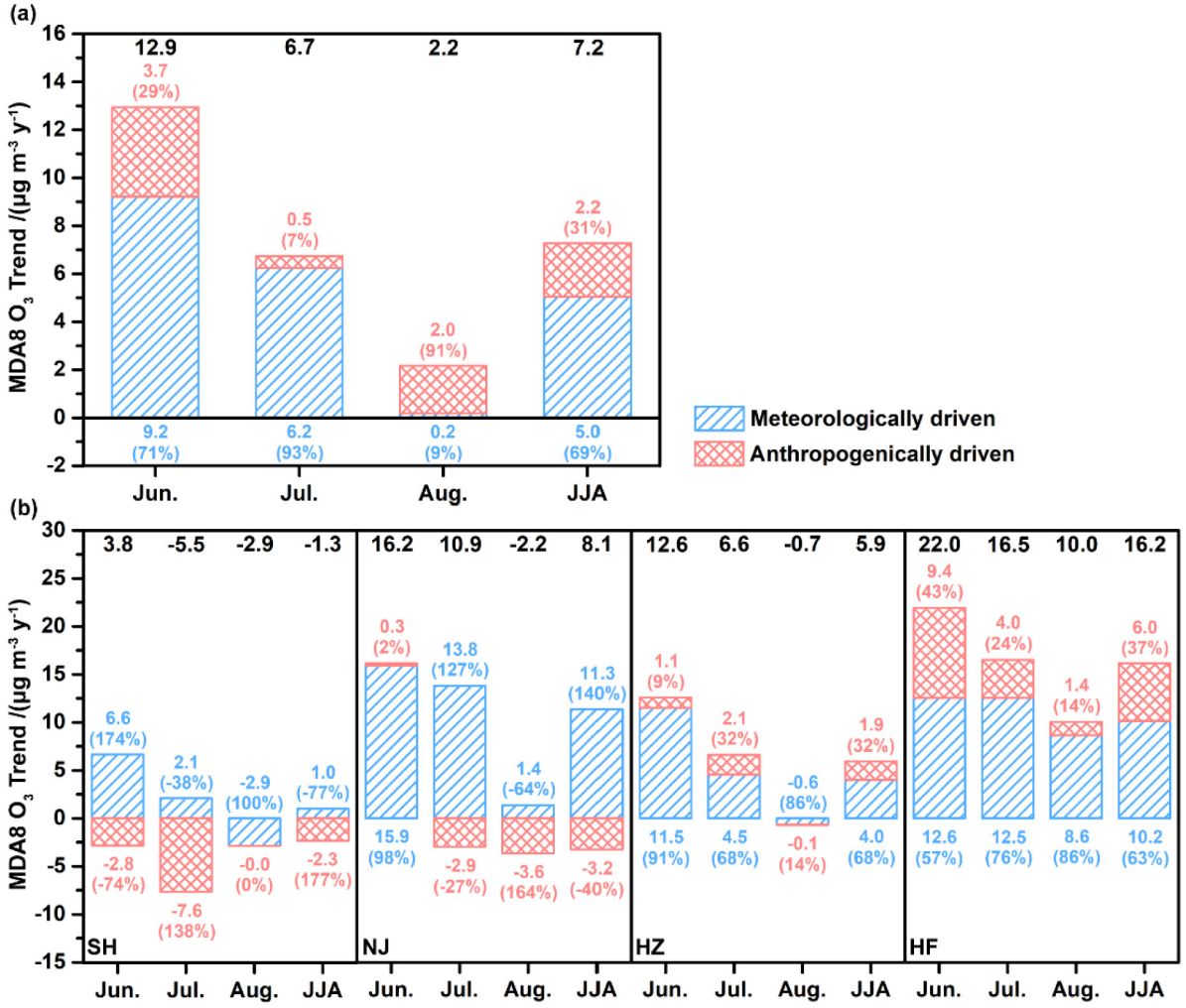

Fig. 11. Observed, meteorologically driven, and anthropogenically driven trends (μg m^{-3} y^{-1}) of MDA8 O_3 concentrations in June, July, August, and JJA over 2015–2019 in (a) the whole of YRD and (b) four cities (Shanghai, Nanjing, Hangzhou, and Hefei). Black values represent observed trends; blue bars and values represent meteorologically driven trends; pink bars and values represent anthropogenically driven trends. The blue and pink values in parentheses represent the contributions (%) of 2015–2019 changes in meteorological factors and anthropogenic emissions to the observed trends, respectively.

4. Conclusions and discussions

Previous observational and modeling studies generally presented region-based estimates of the meteorological impacts on daily or yearly variations of MDA8 O_3. In this work, we paid special attention to the meteorological impacts at city scale. The meteorological impacts on MDA8 O_3 were quantified by the MLR approach and the relative contributions of key meteorological parameters that led to the observed daily variations of MDA8 O_3 were obtained by the LMG method. We compared results for individual cities (Shanghai, Nanjing, Hangzhou, and Hefei) for individual months (June, July, and August) with those for YRD and JJA to investigate the spatiotemporal heterogeneity in quantifying the meteorological effects and to make suggestions for air quality planning.

The statistics showed that the changes in key meteorological parameters could explain 72%, 56%, 58%, 64%, and 58% of observed daily variations of MDA8 O_3 in JJA in YRD, Shanghai, Nanjing, Hangzhou, and Hefei, respectively. RH was found to be the top driver that explained 33%–84% of the daily variations in MDA8 O_3 explained by key meteorological parameters in YRD and four cities. Compared to MDA8O_3_MLR of YRD, MDA8O_3_MLR of the local cities always had higher correlation coefficients with MDA8O_3_OBS and lower MBs and NMBs over 2015–2020. The fitted MLR equations of the local city also had better performance in capturing summertime O_3-polluted days than those of YRD; the fitted MLR equations of the local city (of YRD) captured 54% (17%), 63% (51%), and 52% (27%) of the observed O_3-polluted days in JJA of 2015–2020 in Shanghai, Nanjing, and Hangzhou, respectively.

The meteorologically driven trends (Trend_Met) were calculated using the established MLR equations. Over 2015–2019, Trend_Obs and Trend_Met were mostly positive in YRD, Nanjing, Hangzhou, and Hefei, considering the trends of MDA8 O_3 in JJA or in individual months (June, July, August). Trend_Met were estimated to contribute 69%, −77%, 140%, 68%, and 63% to Trend_Obs of JJA in YRD, Shanghai, Nanjing, Hangzhou, and Hefei, respectively. In Shanghai/Nanjing, Trend_Obs, Trend_Met, and assumed anthropogenically driven trend of JJA over 2015–2019 were $-1.3/+8.1$ μg m^{-3} y^{-1}, $+1.0/+11.3$ μg m^{-3} y^{-1}, and $-2.3/-3.2$ μg m^{-3} y^{-1}, respectively, indicating that changes in anthropogenic emission were estimated to improve ozone pollution by using MLR equations at city scale. Again, RH was found to be the most dominant meteorological parameter that was responsible for Trend_Met in YRD and in four cities over 2015–2019.

The MLR equations obtained from 2015 to 2019 were found to be able to reproduce MDA8 O_3 in 2020. The correlation coefficients of MDA8O_3_MLR in 2020 with observations over JJA were 0.80, 0.55, 0.73, 0.67, and 0.74 for daily variations of MDA8 O_3 in YRD, Shanghai, Nanjing, Hangzhou, and Hefei, respectively. MLR equations captured the decreases in MDA8 O_3 in the whole of YRD in 2020 relative to 2019. Relative to 2019, averaged over JJA, meteorological fields in 2020 reduced MDA8 O_3 by 27.7, 15.4, 49.3, 26.9, and 47.4 μg m^{-3} in YRD, Shanghai, Nanjing, Hangzhou, and Hefei, respectively, while the observed decreases in MDA8 O_3 in 2020 were 20.1, 12.4, 26.5, 30.0, and 40.6 μg m^{-3} at these locations respectively. The top two meteorological parameters driving these changes in MDA8 O_3 were the increases in RH and WS in YRD, Nanjing, and Hangzhou and the increases in RH and EW in Shanghai and Hefei.

Our results show that meteorological conditions play considerably important roles in driving daily and yearly changes in summertime O_3 and the characteristics of which vary by cities and months. Our results suggest that it is necessary to establish MLR equations at city scale to account for the role of meteorology in the control of O_3 pollution. MLR equations can be applied to predict whether meteorology is conducive to O_3 pollution or not on daily or yearly basis if meteorological parameters can be predicted. It should be noted that the fundamental reasons of air pollution are anthropogenic emissions. Fully consideration of the joint influences of emissions and meteorology is needed in air quality management.

In this work, we were focused on the meteorological influences on variations and trends of O_3 in cities in YRD for summer months. Our suggested approach of quantification for cities can be applied in other regions and months. Our conclusions were obtained on the basis of observed MDA8 O_3 concentrations and MERRA-2 reanalysis meteorological data. Analyses can also be conducted in future studies by using observed meteorological data or higher resolution meteorological fields (such as European Centre for Medium-Range Weather Forecasts Reanalysis v5.0 data).

CRediT authorship contribution statement

Jing Qian: Conceptualization, Investigation, Formal analysis, Visualization, Writing - original draft. **Hong Liao:** Conceptualization, Supervision, Funding acquisition, Writing - review & editing. **Yang Yang:** Software, Writing - review & editing, Validation. **Ke Li:** Writing - review & editing, Validation. **Lei Chen:** Writing - review & editing, Validation. **Jia Zhu:** Writing - review & editing.

Data availability

Hourly surface O_3 observations are available at https://quotsoft.net/air/ (Wang, 2021; last access: 8 November 2021). The MERRA-2 reanalysis meteorological data is openly accessible through http://geoschemdata.wustl.edu/ExtData/GEOS_0.5x0.625_AS/MERRA2/ (last access: 8 November 2021).

Declaration of competing interest

The authors declare that they have no known competing financial interests or personal relationships that could have appeared to influence the work reported in this paper.

Acknowledgments

This work was supported by the National Natural Science Foundation of China (grant no. 42021004) and the National Key Research and Development Program of China (grant no. 2019YFA0606804).

Appendix A. Supplementary data

Supplementary data to this article can be found online at https://doi.org/10.1016/j.scitotenv.2022.155107.

References

Chang, L.Y., Xu, J.M., Tie, X.X., Gao, W., 2019. The impact of climate change on the Western Pacific subtropical high and the related ozone pollution in ShanghaiChina. Sci. Rep. 9, 16998. https://doi.org/10.1038/s41598-019-53103-7.

Chinese Ministry of Ecology and Environment, 2013. Technical regulation for ambient air quality assessment (on trial) (in Chinese). available at: https://www.mee.gov.cn/gkml/hbb/bgg/201309/t20130925_260801.htm (last access: 8 November 2021).

Che, H.Z., Gui, K., Xia, X.G., Wang, Y.Q., Holben, B.N., Goloub, P., Cuevas-Agulló, E., Wang, H., Zheng, Y., Zhao, H.J., Zhang, X.Y., 2019. Large contribution of meteorological factors to inter-decadal changes in regional aerosol optical depth. Atmos. Chem. Phys. 19 (16), 10497–10523. https://doi.org/10.5194/acp-19-10497-2019.

Chen, L., Zhu, J., Liao, H., Yang, Y., Yue, X., 2020a. Meteorological influences on PM2.5 and O3 trends and associated health burden since China's clean air actions. Sci. Total Environ. 744, 140837. https://doi.org/10.1016/j.scitotenv.2020.140837.

Chen, X., Zhong, B.Q., Huang, F.X., Wang, X.M., Sarkar, S., Jia, S.G., Deng, X.J., Chen, D.H., Shao, M., 2020b. The role of natural factors in constraining long-term tropospheric ozone trends over Southern China. Atmos. Environ. 220, 117060. https://doi.org/10.1016/j.atmosenv.2019.117060.

Dang, R.J., Liao, H., Fu, Y., 2021. Quantifying the anthropogenic and meteorological influences on summertime surface ozone in China over 2012–2017. Sci. Total Environ. 754, 142394. https://doi.org/10.1016/j.scitotenv.2020.142394.

Gong, C., Liao, H., 2019. A typical weather pattern for ozone pollution events in North China. Atmos. Chem. Phys. 19 (22), 13725–13740. https://doi.org/10.5194/acp-19-13725-2019.

Grömping, U., 2006. Relative importance for linear regression in R: the package relaimpo. J. Stat. Softw. 17, 1–27. https://doi.org/10.18637/jss.v017.i01.

Han, H., Liu, J., Shu, L., Wang, T.J., Yuan, H.L., 2020. Local and synoptic meteorological influences on daily variability in summertime surface ozone in eastern China. Atmos. Chem. Phys. 20 (1), 203–222. https://doi.org/10.5194/acp-20-203-2020.

Jacob, D.J., Winner, D.A., 2009. Effect of climate change on air quality. Atmos. Environ. 43 (1), 51–63. https://doi.org/10.1016/j.atmosenv.2008.09.051.

Johnson, C.E., Collins, W.J., Stevenson, D.S., Derwent, R.G., 1999. Relative roles of climate and emissions changes on future tropospheric oxidant concentrations. J. Geophys. Res. 104 (D15), 18631–18645. https://doi.org/10.1029/1999jd900204.

Kutner, M., Nachtsheim, C., Neter, J., 2004. Applied Linear Regression Models. Richard D. Irwin, Inc, Homewood, Illinois.

Li, K., Jacob, D.J., Liao, H., Shen, L., Zhang, Q., Bates, K.H., 2019a. Anthropogenic drivers of 2013–2017 trends in summer surface ozone in China. Proc. Natl. Acad. Sci. U. S. A. 116 (2), 422–427. https://doi.org/10.1073/pnas.1812168116.

Li, K., Jacob, D.J., Liao, H., Zhu, J., Shah, V., Shen, L., Bates, K.H., Zhang, Q., Zhai, S.X., 2019b. A two-pollutant strategy for improving ozone and particulate air quality in China. Nat. Geosci. 12, 906–911. https://doi.org/10.1038/s41561-019-0464-x.

Li, K., Jacob, D.J., Shen, L., Lu, X., De Smedt, I., Liao, H., 2020. Increases in surface ozone pollution in China from 2013 to 2019: anthropogenic and meteorological influences. Atmos. Chem. Phys. 20 (19), 11423–11433. https://doi.org/10.5194/acp-20-11423-2020.

Liu, Y.M., Wang, T., 2020. Worsening urban ozone pollution in China from 2013 to 2017–Part 1: the complex and varying roles of meteorology. Atmos. Chem. Phys. 20 (11), 6305–6321. https://doi.org/10.5194/acp-20-6305-2020.

Otero, N., Sillmann, J., Mar, K.A., Rust, H.W., Solberg, S., Andersson, C., Engardt, M., Bergström, R., Bessagnet, B., Colette, A., Couvidat, F., Cuvelier, C., Tsyro, S., Fagerli, H., Schaap, M., Manders, A., Mircea, M., Briganti, G., Cappelletti, A., Adani, M., D'Isidoro, M., Pay, M.T., Theobald, M., Vivanco, M.G., Wind, P., Ojha, N., Raffort, V., Butler, T., 2018. A multi-model comparison of meteorological drivers of surface ozone over Europe. Atmos. Chem. Phys. 18 (16), 12269–12288. https://doi.org/10.5194/acp-18-12269-2018.

Shen, L., Mickley, L.J., Tai, A.P.K., 2015. Influence of synoptic patterns on surface ozone variability over the eastern United States from 1980 to 2012. Atmos. Chem. Phys. 15 (19), 10925–10938. https://doi.org/10.5194/acp-15-10925-2015.

Tu, J., Xia, Z.G., Wang, H.S., Li, W.Q., 2007. Temporal variations in surface ozone and its precursors and meteorological effects at an urban site in China. Atmos. Res. 85 (3–4), 310–337. https://doi.org/10.1016/j.atmosres.2007.02.003.

Wang, X.L, 2021. Historical air quality data in China. available at: https://quotsoft.net/air, last access: 8 November 2021.

Xie, F.J., Lu, X.B., Yang, F., Li, W.Q., Li, J., Xie, Y.S., Wang, Y., Liu, Y.H., Wang, Q.J., Hu, J.L., 2021. Transport influence and potential sources of ozone pollution for Nanjing during spring and summer in 2017 (in Chinese). Environ. Sci. 42 (1), 88–96. https://doi.org/10.13227/j.hjkx.202005077.

Xu, L., Pierce, D.W., Russell, L.M., Miller, A.J., Somerville, R.C.J., Twohy, C.H., Ghan, S.J., Singh, B., Yoon, J.H., Rasch, P.J., 2015. Interannual to decadal climate variability of sea salt aerosols in the coupled climate model CESM1.0. J. Geophys. Res. Atmos. 120 (4), 1502–1519. https://doi.org/10.1002/2014JD022888.

Yang, L.F., Luo, H.H., Yuan, Z.B., Zheng, J.Y., Huang, Z.J., Li, C., Lin, X.H., Louie, P.K.K., Chen, D.H., Bian, Y.H., 2019. Quantitative impacts of meteorology and precursor emission changes on the long-term trend of ambient ozone over the Pearl River Delta, China, and implications for ozone control strategy. Atmos. Chem. Phys. 19 (20), 12901–12916. https://doi.org/10.5194/acp-19-12901-2019.

Yang, Y., Russell, L.M., Xu, L., Lou, S.J., Lamjiri, M.A., Somerville, R.C.J., Miller, A.J., Cayan, D.R., DeFlorio, M.J., Ghan, S.J., Liu, Y., Singh, B., Wang, H.L., Yoon, J.H., Rasch, P.J., 2016. Impacts of ENSO events on cloud radiative effects in preindustrial conditions: changes in cloud fraction and their dependence on interactive aerosol emissions and concentrations. J. Geophys. Res. Atmos. 121 (11), 6321–6335. https://doi.org/10.1002/2015JD024503.

Yin, P., Chen, R.J., Wang, L.J., Meng, X., Liu, C., Niu, Y., Lin, Z.J., Liu, Y.N., Liu, J.M., Qi, J.L., You, J.L., Zhou, M.G., Kan, H.D., 2017. Ambient ozone pollution and daily mortality: a nationwide study in 272 Chinese cities. Environ. Health Perspect. 125 (11), 117006. https://doi.org/10.1289/EHP1849.

Yue, X., Unger, N., Harper, K., Xia, X.G., Liao, H., Zhu, T., Xiao, J.F., Feng, Z.Z., Li, J., 2017. Ozone and haze pollution weakens net primary productivity in China. Atmos. Chem. Phys. 17 (9), 6073–6089. https://doi.org/10.5194/acp-17-6073-2017.

Zhai, S.X., Jacob, D.J., Wang, X., Shen, L., Li, K., Zhang, Y.Z., Gui, K., Zhao, T.L., Liao, H., 2019. Fine particulate matter (PM2.5) trends in China, 2013–2018: separating contributions from anthropogenic emissions and meteorology. Atmos. Chem. Phys. 19 (16), 11031–11041. https://doi.org/10.5194/acp-19-11031-2019.